

# Enhanced nematic fluctuations near an antiferromagnetic Mott insulator and possible application to high- $T_c$ cuprates

Peter P. Orth,<sup>1</sup> Bhilahari Jeevanesan,<sup>2</sup> Rafael M. Fernandes,<sup>3</sup> and Jörg Schmalian<sup>2,4</sup>

<sup>1</sup>*Department of Physics and Astronomy, Iowa State University, Ames, Iowa 50011, USA*

<sup>2</sup>*Institute for Theory of Condensed Matter, Karlsruhe Institute of Technology (KIT), 76131 Karlsruhe, Germany*

<sup>3</sup>*School of Physics and Astronomy, University of Minnesota, Minneapolis, Minnesota 55455, USA*

<sup>4</sup>*Institute for Solid State Physics, Karlsruhe Institute of Technology (KIT), 76131 Karlsruhe, Germany*

Motivated by the widespread experimental observations of nematicity in strongly underdoped cuprate superconductors, we investigate the possibility of enhanced nematic fluctuations in the vicinity of a Mott insulator that displays Néel-type antiferromagnetic order. By performing a strong-coupling expansion of an effective model that contains both Cu- $d$  and O- $p$  orbitals on the square lattice, we demonstrate that quadrupolar fluctuations in the  $p$ -orbitals inevitably generate a biquadratic coupling between the spins of the  $d$ -orbitals. The key point revealed by our classical Monte Carlo simulations and large- $N$  calculations is that the biquadratic term favors local stripe-like magnetic fluctuations, which result in an enhanced nematic susceptibility that onsets at a temperature scale determined by the effective Heisenberg exchange  $J$ . We discuss the impact of this type of nematic order on the magnetic spectrum and outline possible implications on our understanding of nematicity in the cuprates.

## INTRODUCTION

Hole-doped cuprates are susceptible to a variety of different types of electronic order in the underdoped regime. Examples include tendencies towards charge order [1–4], which becomes long-ranged in the presence of large magnetic fields [1, 4], and tendencies towards nematic order [5–10], characterized by the breaking of the tetragonal symmetry of the system [11, 12]. The fact that these tendencies appear in the region of the phase diagram where a pseudogap is also observed (see schematic Fig. 1) suggest a close interplay between these seemingly different phenomena, a topic that remains widely debated in the field (for recent reviews, see [13, 14]).

Although the microscopic mechanisms behind these different ordering tendencies, and particularly of nematicity, remain unsettled, they have been the subject of many different theoretical proposals (see, for instance, [15–30], and also the reviews [11, 12]). While a complete theory for nematicity in the cuprates is beyond the scope of our work, here we show that an important contribution to the nematic susceptibility arises already near the Mott (or more precisely, charge-transfer [31]) insulating state of the parent compound. For the rest of the paper, thus, we focus only on the spin correlations near the Mott state, and neglect other phenomena that are certainly important for a complete description of the hole-doped cuprates, and which may also be important to describe nematicity, such as charge order, pseudogap, time-reversal symmetry-breaking, pair-density waves, and superconductivity [13, 14].

To be more specific, we consider the so-called Emery model [32], an effective model that attempts to capture both Cu and O low-energy degrees of freedom by introducing  $d_{x^2-y^2}$  orbitals on the sites of the square lattice and  $p_x$  ( $p_y$ ) orbitals on the horizontal (vertical) bonds.

Consider first the case where only  $d$ -orbitals are present. In the half-filled Mott insulating state, the charge degrees of freedom are quenched, and the low-energy physics is described completely in terms of an AFM Heisenberg interaction  $J$  between the  $d$ -orbital spins, which ultimately gives rise to a Néel AFM ground state. Upon light hole-doping, the effective Hamiltonian is known as the  $t - J$  model [33]:

$$H_{t-J} = \sum_{ij\alpha} t_{ij} \tilde{d}_{i\alpha}^\dagger \tilde{d}_{j\alpha} + J \sum_{\langle ij \rangle} \left( \mathbf{S}_i \cdot \mathbf{S}_j - \frac{1}{4} n_i n_j \right). \quad (1)$$

Here,  $t_{ij}$  denotes the hole hopping parameters and  $J$  the AFM exchange coupling. The operator  $\mathbf{S}_i = \frac{1}{2} \sum_{\alpha\beta} \tilde{d}_{i\alpha}^\dagger \boldsymbol{\sigma}_{\alpha\beta} \tilde{d}_{i\beta}$  describes the  $d$ -orbital spin and  $n_i = \sum_{\alpha} \tilde{d}_{i\alpha}^\dagger \tilde{d}_{i\alpha}$  the corresponding charge. The strong local Coulomb interaction is incorporated in terms of the hole creation operator  $\tilde{d}_{i\alpha}^\dagger = (1 - n_{i\bar{\alpha}}) d_{i\alpha}^\dagger$ , reflecting the fact that double occupancy of the sites is not allowed near the Mott insulating state.

As we demonstrate below via a strong coupling expansion of the Emery model, the inclusion of the  $p$ -orbitals leads to an important additional term in the  $t - J$  Hamiltonian. While the two terms in Eq. (1) remain the same, albeit with a different microscopic expression for  $J$ , non-critical quadrupolar fluctuations of the  $p$ -orbitals, enhanced by the repulsion between  $p$ -orbitals, generate a positive biquadratic coupling  $K > 0$  between the  $d$ -orbital spins:

$$H_K = -K \sum_i [\mathbf{S}_i \cdot (\mathbf{S}_{i-\hat{x}} + \mathbf{S}_{i+\hat{x}} - \mathbf{S}_{i-\hat{y}} - \mathbf{S}_{i+\hat{y}})]^2, \quad (2)$$

resulting in an effective  $t - J - K$  Hamiltonian,  $H_{t-J-K} = H_{t-J} + H_K$ .

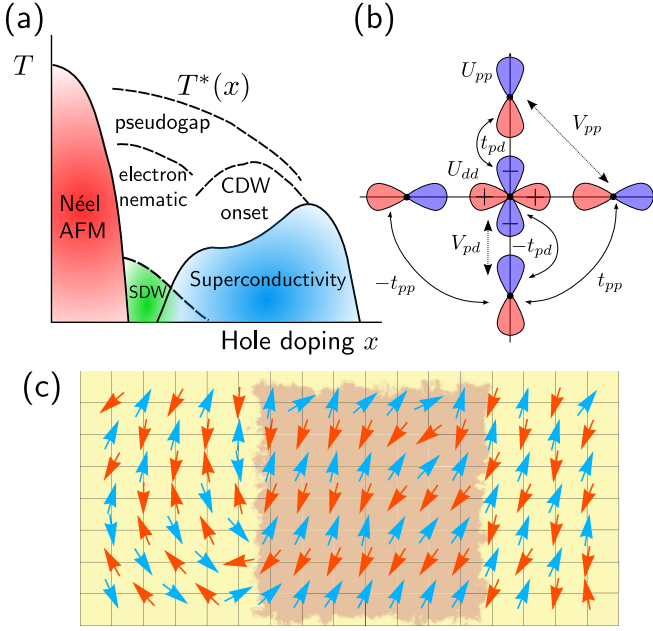


FIG. 1. **Microscopic manifestation of nematic fluctuations.** (a) Schematic phase diagram of hole-doped cuprate superconductors. (b) The microscopic model we use contains a Cu  $3d_{x^2-y^2}$  orbital (center orbital) and O  $2p_x$  and  $2p_y$  orbitals in a single unit cell. The hopping parameters are given by  $t_{pd}, t_{pp}$  and interactions are considered on-site  $U_{dd}, U_{pp}$  and between nearest-neighbors  $V_{pd}, V_{pp}$ . (c) Simple illustration that nematic fluctuations induce a short-ranged magnetic stripe ordered region (light red) within a Néel ordered background (yellow). This snapshot is taken from our classical Monte Carlo simulations. Red and blue color of the arrows denote out-of-the-plane components of the spins.

Using classical Monte Carlo and large- $N$  analytical methods, we find that the main consequence of  $H_K$  is to enhance the static electronic nematic susceptibility  $\chi_{\text{nem}}$  near the AFM-Mott insulating state. However,  $\chi_{\text{nem}}$  is not found to diverge on its own – instead, it peaks at a temperature scale proportional to  $J$ , instead of  $K$ . The location of the peak depends on the relative strength of quantum and thermal fluctuations and shifts towards smaller temperatures for larger quantum fluctuations. As illustrated in Fig. 1(c), the enhancement of nematic fluctuations promoted by  $H_K$  has its origins on the *short-ranged* magnetic stripe ordered regions that this term favors within the (much longer ranged) Néel ordered background. Consequently, within the  $t - J - K$  model, the onset of nematic order requires an additional symmetry breaking field that can take advantage of the enhanced susceptibility. While a more detailed discussion of the application of these results to the cuprates is left to the end of this paper, we note that this mechanism for enhanced nematic susceptibility can in principle be combined with other mechanisms proposed in the literature to yield long-range nematic order. Detailed reviews on the proposed mechanisms for nematicity in cuprates,

both within weak and strong coupling regimes, can be found for instance in Refs. [11, 12].

## RESULTS

*Microscopic model.* Our starting point is the interacting three-orbital Emery model  $H = H_0 + H_U + H_V$  [32]. As depicted in Fig. 1(b), it includes the  $d_{x^2-y^2}$  Cu orbital with creation operator  $d_{i,\sigma}^\dagger$  at Bravais lattice position  $\mathbf{R}_i$  and spin  $\sigma$  as well as the  $p_x$  and  $p_y$  O orbitals with creation operators  $p_{i+\hat{x}/2,\sigma}^\dagger$  and  $p_{i+\hat{y}/2,\sigma}^\dagger$ . The non-interacting part  $H_0$  includes hopping between  $p$ -orbitals with (amplitude  $t_{pp}$ ) and between  $d$ - and  $p$ -orbitals (with amplitude  $t_{pd}$ ). The corresponding sign factors of the hopping elements follow from the phases of the orbitals (see Fig. 1(b)) [32]. In addition,  $H_0$  contains on-site terms where the energy difference between Cu and O orbitals is given as  $\Delta = \varepsilon_p - \varepsilon_d$ . Interactions are included on-site  $H_U = U_{dd} \sum_i n_{i,\uparrow}^d n_{i,\downarrow}^d + \frac{U_{pp}}{2} \sum_{i,u} n_{i+u,\uparrow}^p n_{i+u,\downarrow}^p$  with  $u \in \{\hat{x}/2, \hat{y}/2\}$ , and number operators  $n_{i,\sigma}^d = d_{i,\sigma}^\dagger d_{i,\sigma}$  and  $n_{i+u,\sigma}^p = p_{i+u,\sigma}^\dagger p_{i+u,\sigma}$ . We also consider nearest-neighbor interactions  $H_V = \frac{V_{pp}}{2} \sum_{i,u,u'} n_{i+u}^p n_{i+u'}^p + V_{pd} \sum_{i,u} n_{i,u}^d n_{i+u}^p$  with  $u' \in \{\pm \frac{1}{2}(\hat{x} + \hat{y}), \pm \frac{1}{2}(\hat{x} - \hat{y})\}$  and  $n_i^d = \sum_\sigma n_{i,\sigma}^d$ ,  $n_{i+u}^p = \sum_\sigma n_{i+u,\sigma}^p$ .

The largest energy scales are the local repulsion  $U_{dd}$  between  $d$ -orbitals and the charge-transfer energy  $\Delta$  (with  $U_{dd}$  much larger than  $\Delta$ ), suggesting a strong coupling expansion in small  $t_{ij} \ll \Delta, U_{dd} - \Delta$ . This yields a description in terms of localized  $d$ -orbital spins  $\mathbf{S}_i$  coupled to mobile  $p$ -orbital holes. An expansion up to fourth order in the hopping term  $t_{pd}$  was performed in Ref. [34, 35]. There appear Kondo-like exchange couplings  $\propto \mathbf{S}_i \cdot \mathbf{s}_{i+u_1, i+u_2}$  between the  $d$ - and  $p$ -orbital spin densities  $\mathbf{s}_{i+u_1, i+u_2} = \frac{1}{2} \sum_{\tau, \tau'} p_{i+u_1, \tau}^\dagger \boldsymbol{\sigma}_{\tau\tau'} p_{i+u_2, \tau'}$  [36], the familiar Heisenberg spin exchange term  $J \sum_{\langle i,j \rangle} \mathbf{S}_i \cdot \mathbf{S}_j$  and terms that renormalize the  $p$ -orbital hole dispersion. For details we refer to the Methods section and the Supplementary Information. The Kondo-like terms also modify the hole dispersion as the tunneling process of holes through a  $d$ -orbital becomes spin dependent. For example, tunneling through a background of Néel ordered  $d$ -orbital spins leads to the spin dependent hopping parameters  $t_a = \frac{t_{pd}^2}{2} (\frac{1}{\Delta} + \frac{3}{U_{dd}-\Delta})$  and  $t_b = \frac{t_{pd}^2}{2} (\frac{3}{\Delta} + \frac{1}{U_{dd}-\Delta})$  for holes with spin parallel and antiparallel to the central  $d$ -orbital spin [24]. The hole Fermi surface thus appears at momenta  $\mathbf{k} = (\pm \frac{\pi}{2}, \pm \frac{\pi}{2})$  for small doping  $n_p$ .

Most notably for our considerations, the strong coupling expansion also yields a spin exchange term that depends on the occupation of the intermediate  $p$ -orbital between  $d$ -orbital sites:

$$H_{J'} = -J' \sum_{i,\delta} n_{i+\delta/2}^p \mathbf{S}_i \cdot \mathbf{S}_{i+\delta} \quad (3)$$

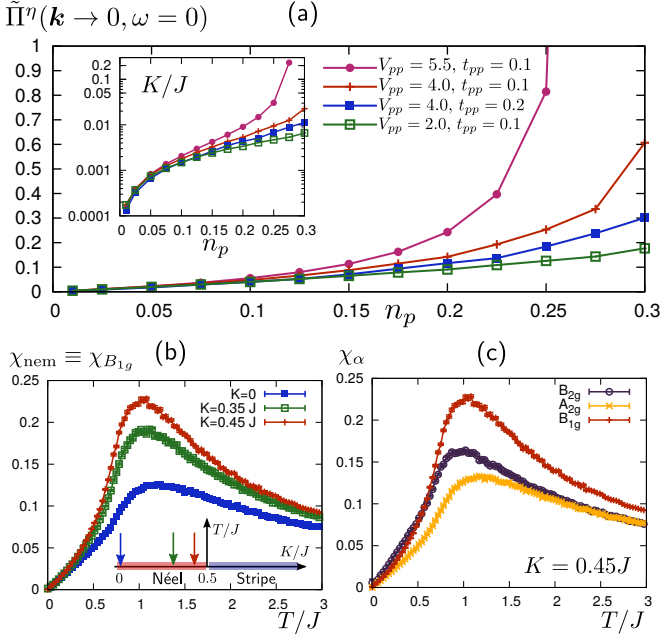


FIG. 2. **Strength of biquadratic exchange  $K$  within Emery model and enhanced nematic spin fluctuations.** (a) Renormalized quadrupolar oxygen density response function  $\tilde{\Pi}_{\mathbf{k}=0}^\eta = \frac{1}{2}[(\Pi_{\mathbf{k}=0}^\eta)^{-1} - U_{\mathbf{k}=0}]^{-1}$  as a function of  $p$ -orbital holes  $n_p$  (per planar  $d$ -orbital) obtained within the three-band Emery model at low temperature  $T = 10^{-2}t_{pp}$  and fixed  $n_d = 1$ . The interaction of the mobile holes with the antiferromagnetic Néel background of  $d$ -orbital spins is fully taken into account. Other parameters are set to  $t_{pd} = 1$ ,  $\Delta = 2.5$ ,  $U_{dd} = 11$  and  $V_{pd} = V_{pp}$  such that  $U_{\mathbf{k}=0} = V_{pp} - \frac{U_{pp}}{8}$ . We use  $U_{pp} = 5.5$  for  $V_{pp} = 5.5$  and  $U_{pp} = 4.5$  for all other values of  $V_{pp}$ . Amplitude of oxygen quadrupolar fluctuations increases with  $V_{pp}$  and smaller oxygen bandwidth, e.g., smaller  $t_{pp}$ . The inset shows the resulting value of  $K/J \propto (J'^2/J)(n_p/t_{pp})$  (at small  $n_p$ ) from which we conclude that an enhancement of the fluctuations by  $V_{pp}$  is crucial for a significant biquadratic exchange coupling. Note that we have approximated  $\Pi_{\mathbf{k}}^\eta \approx \Pi_{\mathbf{k}=0}^\eta$  for simplicity, which does not affect our conclusion. Panels (b-c) show the static nematic susceptibility  $\chi_{\text{nem}}$  in Eq. (7) for the  $H_t$ - $J$ - $K$  model of Eq. (2) at half-filling as a function of temperature  $T$  obtained by Monte Carlo simulations of classical spins. A non-zero  $K$  enhances the response in the nematic  $B_{1g}$  channel only. Inset phase diagram shows that we are investigating  $\chi_{\text{nem}}$  above the Néel ordered state. For consistency with the known spin-wave spectrum, we consider a small ferromagnetic next-nearest-neighbor exchange  $J_2 = -0.1J$ .

where  $\delta \in \{\pm\hat{x}, \pm\hat{y}\}$  and the spin exchange coupling constant is given by  $J' = \sum_{n=0}^3 \frac{t_{pd}^4 \text{sign}(3-2n)}{\Delta^{3-n}(U_{dd}-\Delta)^n}$ . Note that  $J = \sum_{n=0}^2 \frac{t_{pd}^4(4-n^2-\delta_{n,2})}{2\Delta^{3-n}(U_{dd}-\Delta)^n}$  and in the large- $U_{dd}$  limit both are of the same order  $J'/J \rightarrow 1/2$ . Oxygen charge fluctuations thus not only renormalize the Heisenberg exchange via the Kondo coupling terms, but, as we show now, also lead to the biquadratic spin exchange interaction  $K$  in Eq. (2).

We derive the biquadratic exchange  $K$  by first decomposing the  $p$ -orbital densities as  $n_{i+\frac{\hat{z}}{2}}^p = n_i^p + \eta_i$  and  $n_{i+\frac{\hat{y}}{2}}^p = n_i^p - \eta_i$ , where  $\eta_i$  is the quadrupolar (nematic) component of the oxygen charge density [21]. The combination of on-site and nearest-neighbor Coulomb interactions between  $p$ -orbital leads to a term  $(-2 \sum U_{\mathbf{k}} \eta_{\mathbf{k}} \eta_{-\mathbf{k}})$  in the Hamiltonian, where  $U_{\mathbf{k}} = \frac{1}{4}(V_{pp} \text{Re} f_{\mathbf{k}} - \frac{U_{pp}}{2})$  and  $f_{\mathbf{k}} = 1 + e^{-ik_x} + e^{ik_y} + e^{i(k_y - k_x)}$ . Integrating out the quadrupolar charge fluctuations associated with the  $p$ -orbitals (details of this analysis are presented in the Methods section and the Supplementary Information) yields the result for the biquadratic exchange interaction in Eq. (2) with:

$$K = \frac{J'^2}{2} \frac{\int_{\mathbf{k}} \Pi_{\mathbf{k}}^\eta}{1 - (V_{pp} - \frac{U_{pp}}{8}) \Pi_{\mathbf{k}=0}^\eta} > 0. \quad (4)$$

Here,  $\Pi_{\mathbf{k}}^\eta = -\int_{\mathbf{q}, \omega'} \text{Tr}[G_{\mathbf{q}, \omega'}^p(\tau^z \sigma^0 s^0) G_{\mathbf{q}+\mathbf{k}, \omega'}(\tau^z \sigma^0 s^0)]$  is the bare  $p$ -orbital charge susceptibility in the quadrupolar (i.e. nematic) channel. We have used the long-wavelength approximation in the denominator for simplicity (the full expression can be found in the Supplementary Information) and yields qualitatively identical results). The Pauli matrices  $\tau^j$ ,  $s^j$  and  $\sigma^i$  act in orbital ( $p_x, p_y$ ), spin and reduced wavevector  $(\mathbf{k}, \mathbf{k} + (\pi, \pi))$  space, respectively. Note that the presence of the AF background of  $d$ -orbital spins leads to a doubling of the unit cell, and thus  $\int_{\mathbf{q}} \equiv \int_{\text{mBZ}} \frac{d^2 q}{2\pi^2}$  is an integration over the magnetic Brillouin zone (mBZ). Explicit expressions for the  $p$ -orbital Green's functions  $G_{\mathbf{q}, \omega}^p$  are given in the Methods section and the Supplementary Information and yield

$$\Pi_{\mathbf{k}}^\eta = - \int_{\mathbf{q}} \sum_{i,j=1}^4 \frac{v_{ij;\mathbf{q}, \mathbf{q}+\mathbf{k}} \{n_F(\xi_{i,\mathbf{q}}) - n_F(\xi_{j,\mathbf{q}+\mathbf{k}})\}}{\epsilon_{i,\mathbf{q}} - \epsilon_{j,\mathbf{q}+\mathbf{k}}} \quad (5)$$

with  $\epsilon_{i,\mathbf{q}}$  being the renormalized  $p$ -orbital dispersion and  $\xi_{i,\mathbf{q}} = \epsilon_{i,\mathbf{q}} - \mu$  with the chemical potential  $\mu$ . The matrix elements  $v_{ij;\mathbf{q}, \mathbf{q}+\mathbf{k}} = U_{\mathbf{q}}^\dagger(\tau^z \sigma^0) U_{\mathbf{q}-\mathbf{k}}$  contain  $U_{\mathbf{q}}$ , which are unitary matrices that transform between orbital/reduced  $\mathbf{k}$ -space ( $\sigma^i \otimes \tau^j$ ) and band space. Most importantly, Eq. (4) makes it clear that the biquadratic exchange  $K$  in Eq. (2) is a direct consequence of quadrupolar oxygen charge fluctuations. These are a generic feature of the model and exist even if the  $p$ -orbital holes are not dressed by  $d$ -orbital spins.

The oxygen quadrupolar susceptibility  $\Pi_{\mathbf{k}}^\eta$  (and thus  $K$ ) is strictly positive for all  $\mathbf{k}$  and is determined by the occupation number difference between the different oxygen bands. In the relevant regime of small hole fillings  $n_p \ll 1$ , the response approaches a value  $\Pi_{\mathbf{k}=0}^\eta \propto n_p$  at low  $T$ , peaks around  $T \approx |\mu|$  and vanishes as  $1/T$  at large  $T$ . The response increases for smaller bandwidth, e.g., smaller  $t_{pp}$ . This is derived explicitly in

the Supplementary Information for a simpler two-band model that neglects the interaction with the AF background. It also holds true numerically for the full four-band model, as shown in Fig. 2(a), where we present results for the renormalized quadrupolar response  $\tilde{\Pi}_{\mathbf{k}=0}^\eta = \frac{1}{2}[(\Pi_{\mathbf{k}=0}^\eta)^{-1} - U_{\mathbf{k}=0}]^{-1}$  and for the resulting  $K/J$  within the microscopic four-band model. In the calculation we keep  $n_d = 1$ , assuming that holes are doped into the  $p$ -orbitals, but we take the interaction of the mobile holes with the AF background of  $d$ -orbital spins fully into account. We clearly observe that a large nearest-neighbor repulsion  $V_{pp}$  and a small bandwidth  $t_{pp}$  enhance  $K$  (see Eq. (4)). Our results also indicate that an enhancement of the quadrupolar density fluctuations by  $V_{pp}$  is necessary for a significant biquadratic exchange coupling. This follows from  $K/J \propto (J'^2/J)(n_p/t_{pp})$  at small  $n_p$  where  $J' = 0.08$ ,  $J = 0.15$  for the parameters in Fig. 2. Finally, while phonon modes in the same channel are, by symmetry, allowed to give rise to similar behavior, the electronic mechanism for biquadratic exchange is expected to be quantitatively much stronger.

*Enhanced nematic susceptibility.* The implications of  $H_K$  can be better understood in the limit of  $K > J$ . In this case, the AFM ground state is no longer the Néel configuration with ordering vector  $\mathbf{Q} = (\pi, \pi)$ , but the striped configuration with  $\mathbf{Q} = (\pi, 0)$  or  $(0, \pi)$ . While the limit of large  $K/J$  is clearly not realized in the cuprates, it reveals that  $H_K$  supports quantum and classical fluctuations with local striped-magnetic order that have significant statistical weight.

We qualitatively demonstrate this behavior in Fig. 1(c) by showing typical spin configurations of a Monte Carlo analysis of  $H_{t-J-K}$  in the limit of classical spins and where the kinetic energy of the holes is ignored. One clearly sees local striped-magnetic fluctuations (light red background) in an environment of Néel ordered spins (yellow background). Configurations with parallel spins along the  $x$ -axis and along the  $y$ -axis occur with equal probability, hence preserving the tetragonal symmetry of the system. If one, however, weakly disturbs tetragonal symmetry, e.g. by straining one of the axes, this balance is disturbed and one favors striped configurations of one type over the other.

The behavior described above can be quantified in terms of the composite spin variable:

$$\varphi_i = \mathbf{S}_i \cdot (\mathbf{S}_{i-\hat{x}} + \mathbf{S}_{i+\hat{x}} - \mathbf{S}_{i-\hat{y}} - \mathbf{S}_{i+\hat{y}}) \quad (6)$$

which changes sign under a rotation by  $\pi/2$ . Note that the square of this term, which appears in Eq.(2), is invariant under this transformation, and therefore is fully consistent with the four-fold symmetry of the Emery model. While  $\langle \varphi_i \rangle = 0$  for realistic values of  $K$  (and in the absence of external strain), the static nematic susceptibility

$$\chi_{\text{nem}}(T) = \int_0^{1/T} d\tau \sum_i \langle \mathcal{T}_\tau \varphi_i(\tau) \varphi_0(0) \rangle \quad (7)$$

is a measure for the increased relevance of local stripe magnetic configurations. Here,  $\mathcal{T}_\tau$  denotes imaginary time ordering.

We present a quantitative demonstration that the biquadratic exchange  $K$  yields an enhanced nematic susceptibility in the  $B_{1g}$  ( $x^2 - y^2$ ) symmetry channel in Fig. 2(b-c). It contains Monte Carlo results for  $\chi_{\text{nem}}$  for a collection of classical Heisenberg spins that interact according to the  $H_{J-K}$  model. For consistency with the known spin-wave spectrum, we have included an additional small second-neighbor exchange  $J_2 = -0.1J$  in the simulation. One clearly sees that the biquadratic term  $K$  enhances the nematic response in the  $B_{1g}$  channel, corresponding to an inequivalence between the  $x$  and  $y$  axes. In the limit of classical spins, the nematic susceptibility  $\chi_{\text{nem}}(T)$  is non-monotonic, peaking at a temperature governed by the effective exchange interaction of the spins,  $T_{\text{nem}} \sim J$ , which is independent on  $K$ .

The Monte Carlo results also display that  $\chi_{\text{nem}}(T \rightarrow 0) \rightarrow 0$ , which is a consequence of the classical nature of the spins in the simulations and a resulting absence of (thermal) fluctuations in the zero temperature limit. Quantum fluctuations crucially modify this behavior and lead to  $\chi_{\text{nem}}(T \rightarrow 0) > 0$ . This is demonstrated in Fig. 3, where we present results of an analytical calculation of the nematic response  $\chi_{\text{nem}}$  that includes the effect of quantum fluctuations within a soft-spin field-theoretical version of the spin degrees of freedom in Eq. (2). After decoupling the biquadratic exchange term  $K$  in the nematic channel and taking the long wavelength limit, which is appropriate to study the low-energy excitations, we obtain the effective action:

$$S = S_{\text{dyn}} + \int_r \left[ (\nabla \mathbf{n}_r)^2 - \varphi_r \left( (\partial_x \mathbf{n}_r)^2 - (\partial_y \mathbf{n}_r)^2 \right) \right] + \int_r \left[ r_0 \mathbf{n}_r^2 + \frac{u}{2} (\mathbf{n}_r \cdot \mathbf{n}_r)^2 + \frac{\varphi_r^2}{2g} - h_r \varphi_r \right] \quad (8)$$

where  $\mathbf{n}_r$  is the  $N = 3$  component staggered Néel order parameter, as used in the non-linear sigma model of Refs. [37, 38]. The parameter  $r_0$  controls the distance to the AFM Néel quantum critical point located at  $r_{0,c}$ . For  $\delta r_0 \equiv r_0 - r_{0,c} < 0$ , the system has long-range AFM order at  $T = 0$ , whereas for  $\delta r_0 > 0$  it is in the paramagnetic phase (see sketches at the bottom of Fig. 3), and the interaction parameters are  $g \propto K/J > 0$ ,  $u > g$ . The integrations are over  $\int_r \equiv \int_0^{1/T} d\tau \int d^2r$ , where  $r = (\tau, \mathbf{r})$  combines imaginary time  $\tau$  and position  $\mathbf{r} = (x, y)$ . In addition,  $\varphi_r$  is the nematic order parameter of Eq. (6) and  $h_r$  is an external strain field. The quantum dynamics of the Néel order parameter is governed by  $S_{\text{dyn}} = \int_q f(\omega_n) \mathbf{n}_q \cdot \mathbf{n}_{-q}$ , where  $f(\omega_n) \propto \omega_n^2$

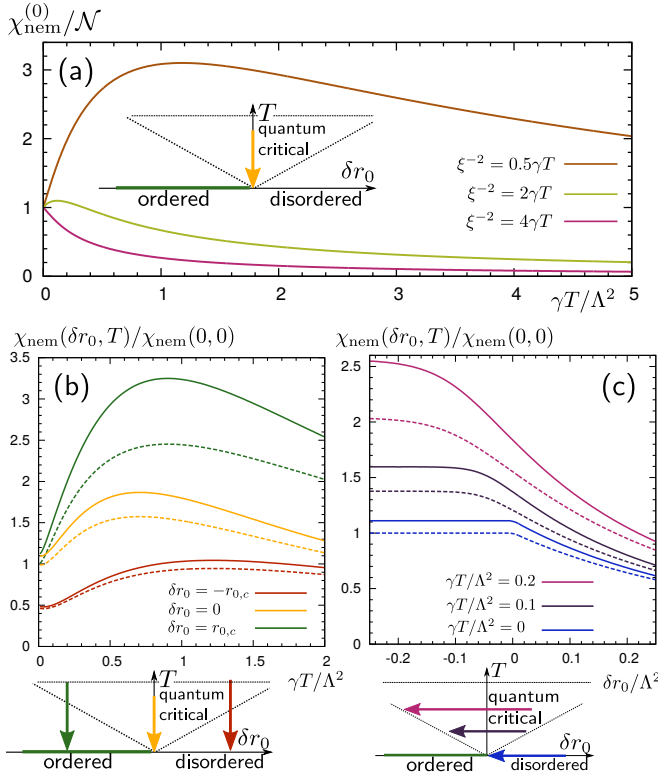


**FIG. 3. Nematic susceptibility including quantum fluctuations.** Effects of quantum fluctuations are included in the analytical treatment of a soft-spin field theory of the  $H_{J-K}$  model. Panel (a) shows the bare nematic susceptibility  $\chi_{\text{nem}}^{(0)}(\xi, T)$  (normalized to its  $T = 0$  value) as a function of temperature  $T$ , right above the Néel QCP  $r_0 = r_{0,c}$  (see inset). Different curves correspond to different functional behavior of the Néel correlation length  $\xi(T)^{-2} = a\gamma T$ . The non-universal constant  $a$  determines whether  $\chi_{\text{nem}}^{(0)}$  peaks at  $T = 0$  ( $a > \pi$ ) or at finite  $T$  ( $a < \pi$ ). Thus,  $\chi_{\text{nem}}^{(0)}$  can exhibit different shapes in different systems, as expected for a non-universal susceptibility, which remains finite at the AFM QCP. Panels (b) and (c) contain results of a large- $N$  treatment of the model, which allows an explicit solution of  $\xi(T, \delta r_0)$ . Dashed (solid) lines are for  $g = 0$  ( $g = 0.1$ ), where  $g \propto K/J$ . Panel (b) is for fixed distances to the QCP  $\delta r_0 = \{-r_{0,c}, 0, r_{0,c}\}$  (green, yellow, red; as indicated in the sketch below) and varying  $T$ . Quantum fluctuations render the susceptibility at  $T = 0$  finite, but have no strong effect on the finite temperature behavior. Importantly, non-zero biquadratic exchange  $g > 0$  enhances the finite temperature nematic response and increases the maximal value of  $\chi_{\text{nem}}$  around  $T \sim \Lambda^2/\gamma \sim J$  (with momentum cutoff  $\Lambda = 10$  and frequency cutoff  $\gamma\Lambda_\omega = 100$ ). Panel (c) is for fixed temperatures  $\gamma T/\Lambda^2 = \{0, 0.1, 0.2\}$  (blue, purple, magenta) and varying  $\delta r_0$ . It demonstrates that the nematic response increases with the magnetic correlation length, as the system approaches the QCP. The quartic coefficient is set to  $u/\gamma = 50$  in (b) and  $u/\gamma = 5$  in (c).

at half filling, while  $f(\omega_n) = \gamma|\omega_n|$  was proposed to describe particle-hole excitations, and will be used below as we describe the system away from half-filling  $n_p > 0$ .

Here,  $q = (\omega_n, \mathbf{q})$  combines Matsubara frequency  $\omega_n$  and momentum  $\mathbf{q}$  (measured relative to the AFM ordering vector  $\mathbf{Q} = (\pi, \pi)$ ) and  $\int_q \equiv T \sum_n \int \frac{d^2 q}{(2\pi)^2}$ .

The nematic susceptibility in Eq. (7) can be obtained for general  $N$  and reads (see Methods section and Supplementary Information):

$$\chi_{\text{nem}} = \frac{\chi_{\text{nem}}^{(0)}}{1 - \frac{g}{N} \chi_{\text{nem}}^{(0)}}, \quad (9)$$

where the bare nematic susceptibility is given by  $\chi_{\text{nem}}^{(0)} = \frac{N}{2} \int_q \frac{|\mathbf{q}|^4 \cos^2(2\theta)}{(\xi^{-2} + |\mathbf{q}|^2 + f(\omega_n))^2}$  with  $\mathbf{q} = |\mathbf{q}|(\cos \theta, \sin \theta)$ . Here,  $\xi$  is the magnetic correlation length for Néel order, that includes interaction corrections and diverges at the AFM phase transition. Right above the quantum critical point at  $\delta r_0 = 0$ , one finds  $\xi^{-2} = a\gamma T$  with non-universal constant  $a$ . As shown in Fig. 3(a), the exact shape of  $\chi_{\text{nem}}^{(0)}(T)$  depends on this non-universal parameter  $a$ , which depends, for example, on the interaction parameter  $u$  or the lattice constant. While  $\chi_{\text{nem}}^{(0)}$  peaks at finite temperatures for  $a < \pi$ , which is similar to the classical case, the maximum occurs at  $T = 0$  for  $a > \pi$ . Note that nematic correlations remain finite ranged at the AFM quantum critical point and universal behavior of  $\chi_{\text{nem}}^{(0)}$  is not guaranteed (in contrast to the AFM susceptibility, which is universal). Being a non-universal quantity, we thus expect that the precise shape of  $\chi_{\text{nem}}^{(0)}$  can be different for different systems.

In order to make analytic progress and calculate  $a(u)$ , or more generally  $\xi(T, \delta r_0)$ , we consider the limit of large  $N$ . This approach led to important insights in both the description of antiferromagnetic correlations of the cuprate parent compounds [38] and of nematic fluctuations of iron-based superconductors [39]. The magnetic correlation length  $\xi$  is determined self-consistently within large- $N$  for a given distance to the AFM quantum critical point  $\delta r_0$ . Despite the similarity between Eq. (9) and the expression for the nematic susceptibility of iron-based superconductors [39], there are very important differences between the two systems. Because the iron pnictides order magnetically in a striped configuration,  $\chi_{\text{nem}}^{(0)}$  diverges when  $\xi \rightarrow \infty$ , which guarantees that a nematic transition takes place already in the paramagnetic state for any  $g > 0$ . However, because our model orders in a Néel configuration,  $\chi_{\text{nem}}^{(0)}$  remains finite even when  $\xi \rightarrow \infty$ . Although long-range nematic order is not present, nematic fluctuations can be significantly enhanced if the biquadratic exchange  $K \propto g$  is sufficiently large.

In Fig. 3(b,c) we show the nematic susceptibility obtained within the large- $N$  approach (see Methods section and Supplementary Information). Like in the Monte Carlo results (see Fig. 2), we observe, in Fig. 3(b), a broad maximum at finite temperatures around  $T \approx J$ , corresponding at  $\delta r_0 = 0$  to  $a < \pi$ . The lattice cutoff  $\Lambda$



plays the role of  $J$  in the continuum model. The effect of  $g$ , and thus of the biquadratic exchange  $K$ , is to enhance the amplitude of the peak (comparing dashed and solid lines). The pronounced peak of  $\chi_{\text{nem}}$  originates from the bare susceptibility  $\chi_{\text{nem}}^{(0)}$ . As discussed above, the bare response is in turn governed by the magnetic correlation length  $\xi$  that is set by  $T/J$ . Notably, at low temperatures, quantum fluctuations render  $\chi_{\text{nem}}$  (and  $\chi_{\text{nem}}^{(0)}$ ) finite, in stark contrast to our MC results for classical spins. Keeping  $T$  fixed and varying the non-thermal tuning parameter  $\delta r_0$ , we observe in Fig. 3(c) that the nematic response increases for an increasing magnetic correlation length, i.e. Néel fluctuations enhance the nematic susceptibility. This follows from the observation that  $\chi_{\text{nem}}(\delta r_0, T)$  is an increasing function for decreasing  $\delta r_0$ .

*Consequences of long-range nematic order.* As we discussed above, the nematic susceptibility does not diverge within our  $H_{J-K}$  model. Nevertheless, it is interesting to study what happens to the magnetic spectrum if nematic order is induced – either by the presence of a small tetragonal-symmetry breaking field  $h$ , which can induce a sizable nematic order parameter  $\varphi \approx \chi_{\text{nem}} h$ , or by combination with other microscopic mechanisms for nematicity. From the action in Eq. (8), we can readily obtain the dynamic spin susceptibility in the presence of nematic order

$$\chi_{\text{AFM}}(\mathbf{Q} + \mathbf{q}, \omega) = \frac{1}{\xi^{-2} + \mathbf{q}^2 - \varphi(q_x^2 - q_y^2) + f(\omega_n)}, \quad (10)$$

Therefore, as shown in Fig. 4, non-zero  $\varphi$  modifies the spin-spin structure factor near the Néel ordering vector  $\mathbf{Q}$  from a circular shape, which preserves tetragonal symmetry, to an elliptical shape, which breaks tetragonal symmetry. In addition, as  $\varphi$  increases, it shifts the maximum of  $\chi_{\text{AFM}}(\mathbf{Q} + \mathbf{q}, \omega)$  from the commensurate  $\mathbf{q} = 0$  value to an incommensurate wavevector  $\mathbf{q}_{\text{IC}} \neq 0$ , with  $\mathbf{q}_{\text{IC}}$  parallel to either the  $x$  axis (if  $\varphi > 0$ ) or to the  $y$  axis (if  $\varphi < 0$ ). Note that a somewhat related mechanism for the incommensurate spin order, based on the  $t - J$  model, was reported in Refs. [40–42]. Previous works have also focused on nematicity arising from a pre-existing incommensurability [28], whereas in our scenario incommensurate magnetic order is a consequence of nematic order, caused by an enhanced nematic susceptibility in the presence of an external symmetry breaking field.

While these effects onset in the paramagnetic phase, the presence of nematic order should also be manifested in the Néel ordered state by the direction of the  $d$ -orbital moments, which would align parallel to either the  $x$  axis or to the  $y$  axis [43]. Within our model, we argue that such an effect would arise in the presence of spin-orbit coupling in the  $p$ -orbitals, which convert an imbalance in the charge of the  $p_x$  and  $p_y$  orbitals into a preferred

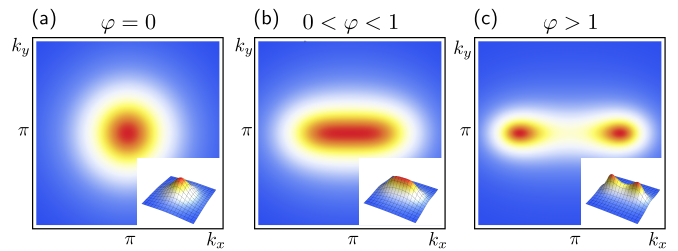


FIG. 4. **Incommensurability transition induced by nematic order.** Panels (a-c) schematically illustrate the effect of finite nematic order  $\varphi$  on the spin-spin correlation function. It shows  $\chi_{\text{AFM}}(\mathbf{k})$  from Eq. (10) (including a fourth order term  $\propto \mathbf{q}^4$ ) for  $\xi^{-2} = 0.2$  and  $\varphi = \{0, 1., 1.5\}$ . In the absence of nematic order ( $\varphi = 0$ ) the magnetic susceptibility peak is isotropic around the Néel ordering vector  $\mathbf{Q} = (\pi, \pi)$ , but non-zero  $0 < \varphi < 1$  leads to an elliptic deformation of the peak. For larger values of  $\varphi > 1$  the peak splits and two incommensurate scattering peaks emerge at  $(\pi \pm \delta, \pi)$ . Note that, within our model, the inequivalence of  $x$  and  $y$  direction appears only in response to an external (or intrinsic) strain field that explicitly breaks  $C_4$  symmetry.

direction for the  $d$ -orbital moment.

At first sight, one might anticipate that  $K$  would affect the spin-wave dispersion of the AFM Néel ground state [44]. As we show in the Supplementary Information, however, the biquadratic exchange of Eq. (2) does not modify the linearized classical spin-wave spectrum. The reason for this peculiar behavior is that the biquadratic exchange annihilates the classical Néel state, i.e. the vacuum of the linear spin wave excitations:

$$H_K |\text{Néel}\rangle = 0. \quad (11)$$

It is important to point out that all results discussed here were obtained considering that the spins of the  $H_{J-K}$  Hamiltonian are treated as vectors, either classical or in the large- $N$  regime. It is interesting to ask what happens if one considers the quantum spin-1/2 case. It turns out that, for spin-1/2, the biquadratic term  $K > 0$  transforms into an AFM next-nearest neighbor bilinear exchange coupling, which certainly changes the spin-wave spectrum. It remains an open question whether the results presented here remain unchanged if one performs this transformation from biquadratic to bilinear exchange in the microscopic model. Importantly, however, we note that a large AFM next-nearest neighbor exchange also favors a stripe magnetic state over a Néel state. Thus, the main ingredient that enhances the nematic susceptibility in the classical spin case seems also to be present in the spin-1/2 case.

## DISCUSSION

In summary, we showed via a strong coupling expansion of the Emery model that quadrupolar charge fluctu-

ations in the  $p$ -orbitals generate a biquadratic exchange coupling between the  $d$ -orbital spins, extending the celebrated  $t - J$  model employed to describe lightly-doped Mott insulators. The main effect of this biquadratic term is to enhance  $B_{1g}$  nematic fluctuations, which however is not translated into a diverging nematic susceptibility. Importantly, the temperature at which the nematic susceptibility peaks is set not by the biquadratic coupling  $K$ , but by the standard nearest-neighbor exchange coupling  $J$ . The peak position is controlled by the relative strength of thermal versus quantum fluctuations, and moves from a temperature of order  $J$  for dominant thermal fluctuations towards zero for dominant quantum fluctuations. The biquadratic exchange  $K$ , however, sets the amplitude of the peak, and both increase for larger values of the repulsion  $V_{pp}$  between nearest-neighbor  $p$ -orbitals.

Thus, our main result is that magnetic correlations associated with the Mott insulating state generate an enhanced nematic susceptibility, which is driven by quadrupolar oxygen density fluctuations. In the remainder of this section, we discuss the possible applications of these results to the nematic tendencies observed in hole-doped cuprates [11, 12]. The mechanism discussed here does not lead to long-range nematic order on its own. However, given the enhanced nematic susceptibility, it is expected that a small tetragonal symmetry-breaking field would lead to a sizable nematic order parameter. Such a symmetry-breaking field is naturally provided by the CuO chains or double chains in  $\text{YBa}_2\text{Cu}_3\text{O}_{7-\delta}$  and  $\text{YBa}_2\text{Cu}_4\text{O}_8$ , respectively. Interestingly, in YBCO, several experimental observations are consistent with the existence of an electronic nematic order parameter [5–7, 10]. Whether the observed nematicity is the result of the intrinsic small symmetry-breaking field combined with a large nematic susceptibility, or the consequence of true long-range order that would onset even if the chains were absent, remains to be determined.

Still in what concerns YBCO, it is interesting to note that nematic order is observed already at rather small doping levels, in the vicinity of the Mott insulating Néel state [6, 45]. In this region of the phase diagram, where our results are the most relevant, the experimental nematic onset temperature is comparable to that of the Néel transition temperature, which in turn is set by  $J$ . Of course, since nematicity is not restricted only to the vicinity of the Néel state, it is possible that there are different mechanisms responsible for nematicity in different regions of the phase diagram [28].

Neutron scattering experiments in YBCO also reveal a strong feedback of nematic order on the magnetic spectrum [6, 43, 45]. In particular, nematic order is manifested as an elliptical spin structure factor centered at the Néel ordering vector. Upon lowering the temperature, the peak splits and gives rise to two unidirectional incommensurate peaks. These observations are qualita-

tively consistent with our results for the effect of nematicity on the AFM magnetic spectrum (see Fig. 4).

To further test the applicability of the effect discussed here on the physics of the cuprates, it would be desirable to directly measure the nematic susceptibility in tetragonal cuprates. In analogy to what has been done for the iron-pnictides (see Ref. [46]),  $\chi_{\text{nem}}$  is closely related to several observables, such as the elastoresistance [47], the shear modulus, or electronic Raman scattering. If the biquadratic term found here was to govern the nematic properties of tetragonal cuprates, such as  $\text{HgBa}_2\text{CuO}_4$ ,  $\chi_{\text{nem}}$  should be enhanced but not divergent – possibly displaying a peak at a temperature comparable to  $J$ . Furthermore, the temperature dependences of  $\chi_{\text{nem}}$  in the  $B_{1g}$  and  $B_{2g}$  channels would be similar, although the former would be larger.

Because the biquadratic term is the result of charge fluctuations on the oxygen  $p$ -orbitals, it is only present in the hole-doped side of the phase diagram, since electron-doping adds charge carriers directly to the Cu sites [48]. To the best of our knowledge, nematic tendencies have not been reported in electron-doped cuprates [11]. It would be interesting to verify this effect by experimentally determining  $\chi_{\text{nem}}$  in tetragonal electron-doped systems, such as  $\text{Nd}_2\text{CuO}_4$ .

## METHODS

### Derivation of $t - J - K$ -model from microscopic three-band model

We derive the biquadratic  $K$  spin exchange term in Eq. (2) from a microscopic interacting three-band model  $H = H_0 + H_U + H_V$  that takes Cu  $d_{x^2-y^2}$  and O  $p_x, p_y$  orbitals into account and reads

$$H_0 = \sum_{i,\sigma} \Delta n_{i\sigma}^p + t_{pd} \sum_{\langle i,j \rangle} ((-1)^{u_{ij}} d_{i\sigma}^\dagger p_{j\sigma} + \text{h.c.}) + t_{pp} \sum_{\langle\langle i,j \rangle\rangle} ((-1)^{u'_{ij}} p_{i\sigma}^\dagger p_{j\sigma} + \text{h.c.}) \quad (12)$$

$$H_U = U_{dd} \sum_i n_{i\uparrow}^d n_{i\downarrow}^d + \frac{U_{pp}}{2} \sum_i n_{i\uparrow}^p n_{i\downarrow}^p \quad (13)$$

$$H_V = V_{pd} \sum_{\langle i,j \rangle} n_i^d n_j^p + V_{pp} \sum_{\langle\langle i,j \rangle\rangle} n_i^p n_j^p. \quad (14)$$

Here,  $d_{i\sigma}^\dagger$  creates a hole in the  $d_{x^2-y^2}$  orbital at Bravais lattice site  $\mathbf{R}_i$ , and  $p_{i\sigma}^\dagger$  creates a hole in the O  $p_x$  and  $p_y$  orbital  $i \equiv \mathbf{R}_i + \frac{\hat{x}}{2}$  and  $i \equiv \mathbf{R}_i + \frac{\hat{y}}{2}$ , respectively (see Fig. 1(b)). The parameters in the Hamiltonian are the on-site orbital energy difference  $\Delta = \epsilon_p - \epsilon_d$ , hoppings  $t_{pp}$ ,  $t_{pd}$  (see Fig. 1), on-site interactions  $U_{pp}$ ,  $U_{dd}$  and nearest-neighbor interactions  $V_{pp}$ ,  $V_{pd}$ .

As  $U_{dd}$  is the largest energy scale, we perform a strong coupling expansion which yields a description in terms of

localized Cu-site spins  $\mathbf{S}_i$  and mobile oxygen holes. The second order terms contain direct O hopping terms and Cu-O Kondo coupling terms. We consider these terms in two complementary limits: (i) assuming an antiferromagnetically ordered background of Cu spins that renormalizes the oxygen bandstructure (main text), and (ii) disregarding both terms which yields a free oxygen dispersion (SI). Both calculations yields qualitatively identical results for quadrupolar response  $\tilde{\Pi}^\eta$  (see Fig. 2(a)) and biquadratic exchange  $K$ . To fourth order appears the Heisenberg exchange interaction term and the exchange interaction term in Eq. (3) that includes the density of the intermediate O orbital. Upon integrating out the O holes this term yields the biquadratic exchange  $K$  term of Eq. (2).

As the theory is quartic in O hole operators, we must first decouple the interaction terms. We perform the decoupling in the channel of the total and relative density of O atoms in a unit cell:  $n_i^p = n_{i+\frac{x}{2}}^p + n_{i+\frac{y}{2}}^p$  and  $\eta_i^p = n_{i+\frac{x}{2}}^p - n_{i+\frac{y}{2}}^p$ . Introducing the vector  $\nu_{\mathbf{k}} = (n_{\mathbf{k}}^p, \eta_{\mathbf{k}}^p)^T$ , where  $n_i^p = \frac{1}{N_L} \sum_{\mathbf{k}} n_{\mathbf{k}}^p e^{i\mathbf{k} \cdot \mathbf{R}_i}$ , the interaction terms read

$$H_{U_{pp}} + H_{V_{pp}} = - \sum_{\mathbf{k}; k_x > 0} \nu_{\mathbf{k}}^\dagger U_{\mathbf{k}}^{-1} \nu_{\mathbf{k}} \quad (15)$$

with interaction matrix

$$U_{\mathbf{k}}^{-1} = \frac{2}{N_L} \begin{pmatrix} -\text{Re } U_{+, \mathbf{k}} & \frac{iV_{pp}}{4} \text{Im } f_{\mathbf{k}} \\ -\frac{iV_{pp}}{4} \text{Im } f_{\mathbf{k}} & \text{Re } U_{-, \mathbf{k}} \end{pmatrix}. \quad (16)$$

Here,  $U_{\pm} = \frac{1}{8}(2V_{pp}f_{\mathbf{k}} \pm U_{pp})$  and  $f_{\mathbf{k}} = 1 + e^{-ik_x} + e^{ik_y} + e^{i(k_y - k_x)}$ . We decouple the interactions using a Hubbard-Stratonovich (HS) transformation, which yields an action that is purely quadratic in O operators, but contains the HS fields  $\Phi_{\mathbf{k}} = (\psi_{\mathbf{k}}, \phi_{\mathbf{k}})$ :

$$S = - \int_{q, q'} \sum_{\substack{\alpha, \alpha' \\ \sigma, \sigma'}} p_Q^\dagger G_{Q, Q'}^{-1} p_{Q'} + \int_q \Phi_q^\dagger U_q \Phi_q. \quad (17)$$

Here,  $Q = (q, \alpha, \sigma)$  combines the Matsubara frequency-momentum index  $q = (iq_n, \mathbf{q})$  with index  $\alpha = x, y$ , which runs over the O orbital index  $p_x, p_y$ , and  $\sigma$ , which denotes spin. The Green's function  $G^{-1}$  contains the Cu spin operators due to the coupling term  $\propto J'$  in Eq. (3), the O hopping terms and the HS variables:  $G^{-1} = G_0^{-1} + G_\Phi^{-1} + G_{J'}^{-1}$ . It is diagonal in spin space, and is in orbital space ( $\tau^\alpha$ ) given by

$$G_0^{-1}(Q, Q') = (iq_n - \Delta + \mu) \mathbb{1} - t_{pp} \text{Re}(h_{\mathbf{q}}) \tau^x + t_{pp} \text{Im}(h_{\mathbf{q}}) \tau^y \quad (18)$$

with  $h_{\mathbf{q}} = 1 - e^{iq_x} - e^{-iq_y} + e^{i(q_x - q_y)}$ . Here we suppress the second-order terms of the strong coupling expansion, which simply renormalize the dispersion. If one considers the motion of O holes in the background of AF ordered Cu spins, as we have done to calculate the results of

Fig. 2(a), the dispersion entering  $G_0^{-1}$  is modified accordingly [24, 49]. The other terms in the Green's function read

$$[G_\Phi^{-1} + G_{J'}^{-1}](Q, Q') = A_0(q - q') \tau^0 + A_z(q - q') \tau^z. \quad (19)$$

Here,  $\tau^0 \equiv \mathbb{1}$  and we have defined the two functions

$$A_0(q - q') = \psi_{q - q'} - \sum_{\mathbf{p}} \mathcal{S}_{\mathbf{p}, \mathbf{q} - \mathbf{q}'} h_n(\mathbf{p}, \mathbf{q}' - \mathbf{q}) \quad (20)$$

$$A_z(q - q') = \phi_{q - q'} - \sum_{\mathbf{p}} \mathcal{S}_{\mathbf{p}, \mathbf{q} - \mathbf{q}'} h_\eta(\mathbf{p}, \mathbf{q}' - \mathbf{q}) \quad (21)$$

with Cu spin bilinear  $\mathcal{S}_{\mathbf{p}, \mathbf{q}} = \mathbf{S}_{\mathbf{p}} \cdot \mathbf{S}_{-\mathbf{p} - \mathbf{q}}$  and lattice functions  $h_{n/\eta}(\mathbf{p}, \mathbf{k}) = \frac{J'}{2} (e^{ip_x} \pm e^{ip_y} + e^{-i(p_x + k_x)} \pm e^{-i(p_y + k_y)})$ , where the upper (lower) sign relates to  $h_n$  ( $h_\eta$ ).

Integrating over the O degrees of freedom results in an action of the form

$$S = \int_q \Phi_q^\dagger U_q \Phi_q - \text{Tr} \ln(-G^{-1}), \quad (22)$$

We expand this expression to second order  $S_2 = \frac{1}{2} \text{Tr}[\{G_0(G_\Phi^{-1} + G_{J'}^{-1})\}^2]$  in order to find

$$S_2 = -\frac{1}{2} \int_q \sum_{\alpha, \alpha'} A_\alpha(q) A_{\alpha'}(-q) \Pi_{-q}^{\alpha\alpha'}, \quad (23)$$

which includes the biquadratic exchange  $K$  term. Here, we have introduced the oxygen density response function

$$\Pi_q^{\alpha\alpha'} = - \int_k \text{Tr}[G_0(k) \tau^\alpha G_0(k + q) \tau^{\alpha'}]. \quad (24)$$

The bare biquadratic exchange constant  $K_0$  is given by the  $zz$ -component of this response function as

$$K_0 = \frac{J'^2}{2} \int_q \Pi_q^{zz}. \quad (25)$$

Note that we write  $\Pi_{\mathbf{q}}^{zz} \equiv \Pi_{\mathbf{q}}^\eta$  in the main text. It is straightforward to obtain the biquadratic exchange renormalized by O density fluctuations by performing the Gaussian integration over the HS fields in Eq. (22), which yields the renormalized response function

$$\tilde{\Pi}_{\mathbf{q}}^{\alpha\alpha'} = \Pi_{\mathbf{q}}^{\alpha\alpha'} + \frac{1}{2} \sum_{\beta, \beta'} (\tilde{U}_{\mathbf{q}}^{-1})_{\beta\beta'} \Pi_{\mathbf{q}}^{\beta\alpha} \Pi_{\mathbf{q}}^{\beta'\alpha'} \quad (26)$$

where we have defined  $(\tilde{U}_{\mathbf{q}}) = (U_{\mathbf{q}})_{\alpha\alpha'} - \frac{1}{2} \Pi_{\mathbf{q}}^{\alpha\alpha'}$ . Approximating the local response by the long-wavelength  $\mathbf{q} = 0$  component  $\tilde{\Pi}_{ii}^{zz} \approx \tilde{\Pi}_{\mathbf{q}=0}^{zz}$  yields for renormalized biquadratic exchange constant  $K$  as given in Eq. (4) of the main text.



### Nematic susceptibility within soft-spin quantum field theory

In the main text, we analyze the nematic susceptibility  $\chi_{\text{nem}}$  in the  $t$ - $J$ - $K$ -model using a soft-spin quantum field theory. This allows us to investigate the effect of quantum fluctuations on the nematic response. Our main results are shown in Fig. 3. After decoupling the bi-quadratic  $K$  term using HS variable  $\varphi_r$  the soft-spin action reads

$$S = \gamma \int_q \left[ r_0 + q^2 + (\varphi_r + h_\varphi)(q_x^2 - q_y^2) + \gamma |\omega_n|^{\frac{z}{2}} \right] M_q^\alpha M_{-q}^\alpha + \frac{\gamma^2 u}{2N} \int_{q_1, q_2, q_3} M_{q_1}^\alpha M_{q_2}^\alpha M_{q_3}^\beta M_{-q_1 - q_2 - q_3}^\beta + \int_r \frac{N \varphi_r}{2g} \quad (27)$$

Here,  $\mathbf{M}_q$  denotes an  $N$ -component Néel magnetization order parameter ( $N = 3$  in the physical system) and summation over repeated indices  $\alpha, \beta$  is implied. The integrations are over  $\int_r = \int_0^{1/T} d\tau \int d^2r$  and  $\int_q = T \sum_{\omega_n} \int^\Lambda \frac{d^2q}{(2\pi)^2}$  up to some dimensionless momentum and frequency cutoffs  $\Lambda$  and  $\gamma\Lambda_\omega$ . The parameter  $r_0$  controls the distance to the quantum critical point separating a Néel ordered regime from a quantum disordered paramagnetic regime,  $u$  is an interaction constant and the coupling constant  $g \propto K/J$  is proportional to the biquadratic exchange. We have added a source field  $h_\varphi \equiv h_r$  that couples to homogeneous nematic order. We use a dynamic critical exponent of  $z = 2$  in the following, which describes damping due to particle-hole excitations in the presence of mobile holes.

The nematic susceptibility in Eq. (7) can be calculated from the partition function  $Z = \int \mathcal{D}(\mathbf{M}_q, \varphi_r) e^{-S}$  as

$$\chi_{\text{nem}} = \frac{T}{L^2} \frac{\partial^2 Z}{\partial h_\varphi^2} \Big|_{h_\varphi=0} = \frac{\chi_{\text{nem},0}}{1 - \frac{g}{N} \chi_{\text{nem},0}} \quad (28)$$

where  $L$  is the linear system size and the bare nematic susceptibility is given by

$$\chi_{\text{nem},0} = \frac{N}{g} - \frac{T}{L^2 \langle \bar{\varphi}_r^2 \rangle}, \quad (29)$$

with  $\bar{\varphi}_r = \varphi_r + h_\varphi$ . In the following, we consider homogeneous HS fields  $\varphi_r, \bar{\varphi}_r$ . To calculate the expectation value  $\langle \bar{\varphi}_r^2 \rangle$ , we first decouple the quartic  $u$ -term in Eq. (27) using HS field  $\psi$ , then separate longitudinal and transverse components  $\mathbf{M}_r = (\sqrt{N}M, \boldsymbol{\pi}_r)$  and integrate over the transverse ones to arrive at the (dimensionless) action  $s \equiv S/[L^2(\gamma T)^{-1}]$  given by

$$s = NrM^2 + \frac{N(\bar{\varphi}_r - h_\varphi)^2}{2\tilde{g}} - \frac{\psi^2}{2\tilde{u}} + \frac{N-1}{2} \gamma \int_q \ln \left( r_q + \bar{\varphi}_r(q_x^2 - q_y^2) \right) \quad (30)$$

Here,  $r_q = r + q^2 + \gamma|\omega_n|$ ,  $r = r_0 + \psi$  and we have defined dimensionless interaction constants  $\tilde{g} = g/\gamma$  and  $\tilde{u} = u/\gamma$ . Next, we expand the logarithm in small  $\bar{\varphi}_r$  up to second order and obtain Eq. (29) by differentiation as

$$\chi_{\text{nem},0} = \frac{NT}{2} \sum_{\omega_n} \int^\Lambda \frac{d^2q}{(2\pi)^2} \frac{q^4 \cos^2(2\theta)}{(r + q^2 + \gamma|\omega_n|)^2} \quad (31)$$

We can exactly perform the summation over Matsubara frequencies, the momentum integration and then absorb the cutoff  $\Lambda$  by expressing  $\chi_{\text{nem},0}$  in terms of the dimensionless variables  $\tilde{T} = \gamma T/\Lambda^2$  and  $\tilde{r} = r/\Lambda^2$ . The lengthy expression is given in the Supplemental Material [49] together with a three-dimensional plot as a function of  $\tilde{T}$  and  $\tilde{r}$ . Cuts for different functional behaviors of the magnetic Néel correlation length on temperature  $r(T) \equiv \xi^{-2}(T)$  are shown in Fig. 3(a).

We can derive the functional behavior of  $r(T)$  within a large- $N$  approach, where we need to solve the following well-known self-consistency equation

$$r = r_0 + uM^2 + \frac{u}{2} \int_q \frac{1}{r + q^2 + \gamma|\omega_n|} \quad (32)$$

Solving this equation requires us to introduce a finite frequency cutoff  $\Lambda_\omega$ , but the qualitative behavior of  $\chi_{\text{nem},0}$  and  $\chi_{\text{nem}}$  does not depend on the cutoff choice as long as  $\Lambda, \Lambda_\omega \gg r, \gamma T$ . The results for  $\chi_{\text{nem},0}$  and  $\chi_{\text{nem}}$  shown in Fig. 3(b, c) are obtained from the large- $N$  solution of  $r(T)$  for fixed parameters  $\tilde{u}, \Lambda, \Lambda_\omega$  and distance to the quantum-critical point  $\delta r_0 = r - r_{0,c}$ .

### Details on the classical Monte-Carlo simulations

The Monte Carlo simulations were carried out at 100 equally spaced temperature points in the interval  $0.001 < T/J < 2.971$ . We applied a combination of single-move Metropolis Monte Carlo steps and non-local parallel-tempering-exchange steps between neighboring temperature configurations. The simulations shown in Fig. 2(b, c) of the main text were carried out for systems of  $40 \times 40$  spins and biquadratic exchange couplings  $K/J = \{0.0, 0.35, 0.45\}$ . We consider a ferromagnetic next-nearest-neighbor exchange coupling  $J_2 = -0.1J$  as well. Note that the ground state phase transition in the classical model between Néel and collinear order occurs at  $J/2 = J_2 + K$ . Following thermalization, the averages were computed for each temperature with at least  $4.5 \times 10^6$  Monte Carlo sweeps (MCS). The error bars were estimated by using the well-known Jackknife procedure.

Finally, we mention that we have performed Monte-Carlo simulations also for the purely bilinear spin Hamiltonian that is obtained from  $H_{J-K}$  by using the well-known relations valid for spin-1/2 operators:  $(\mathbf{S}_i \cdot \mathbf{S}_j)^2 = \frac{3}{16} - \frac{1}{2} \mathbf{S}_i \cdot \mathbf{S}_j$  and  $(\mathbf{S}_i \cdot \mathbf{S}_j)(\mathbf{S}_i \cdot \mathbf{S}_k) = \frac{1}{4} \mathbf{S}_j \cdot \mathbf{S}_k + \frac{i}{2} \mathbf{S}_i \cdot$

$(\mathbf{S}_j \times \mathbf{S}_k)$ . These allow rewriting the biquadratic  $K$  term as a sum of three *bilinear* spin exchange terms

$$\begin{aligned} \tilde{H}_{J-K} = & \frac{1}{2} \left( J + \frac{K}{4S^2} \right) \sum_i \sum_{\delta} \mathbf{S}_i \cdot \mathbf{S}_{i+\delta} \\ & + \frac{K}{8S^2} \sum_i \sum_{\delta'} \mathbf{S}_i \cdot \mathbf{S}_{i+\delta'} - \frac{K}{16S^2} \sum_i \sum_{\delta''} \mathbf{S}_i \cdot \mathbf{S}_{i+\delta''}. \end{aligned} \quad (33)$$

Here,  $\delta(\delta')$  runs over the (next-)nearest neighbors of the square lattice and  $\delta''$  runs over the second-neighbors along the bonds. Importantly, classical Monte-Carlo simulation results for this Hamiltonian  $\tilde{H}_{J-K}$  show the same enhancement of the nematic susceptibility  $\chi_{\text{nem}}$  as a function of  $K$  as results for the original Hamiltonian  $H_{J-K}$  that includes the biquadratic exchange term.

### ACKNOWLEDGMENTS

We gratefully acknowledge helpful discussions with A. V. Chubukov, M.-H. Julien, B. Keimer, M. Le Tacon, and L. Taillefer.

### COMPETING INTERESTS

The authors declare no competing interests.

### AUTHOR CONTRIBUTIONS

P.P.O., B.J., R.M.F. and J.S. contributed extensively to the calculations, prepared the figures and wrote the paper.

### FUNDING

P.P.O. acknowledges support from Iowa State University Startup Funds. J.S. acknowledges financial support by the Deutsche Forschungsgemeinschaft through Grant No. SCHM 1031/7-1. This work was carried out using the computational resource bwUniCluster funded by the Ministry of Science, Research and Arts and the Universities of the State of Baden-Württemberg, Germany, within the framework program bwHPC.

### DATA AVAILABILITY

The data that support the findings of this study are available from the authors upon request.

- [1] Wu, T. *et al.* Magnetic-field-induced charge-stripe order in the high-temperature superconductor  $\text{YBa}_2\text{Cu}_3\text{O}_y$ . *Nature* **477**, 191–194 (2011).
- [2] Ghiringhelli, G. *et al.* Long-range incommensurate charge fluctuations in  $(\text{Y, Nd})\text{Ba}_2\text{Cu}_3\text{O}_{6+x}$ . *Science* **337**, 821–825 (2012).
- [3] Chang, J. *et al.* Direct observation of competition between superconductivity and charge density wave order in  $\text{YBa}_2\text{Cu}_3\text{O}_{6.67}$ . *Nat. Phys.* **8**, 871–876 (2012).
- [4] LeBoeuf, D. *et al.* Thermodynamic phase diagram of static charge order in underdoped  $\text{YBa}_2\text{Cu}_3\text{O}_y$ . *Nat. Phys.* **9**, 79–83 (2012).
- [5] Ando, Y., Segawa, K., Komiya, S. & Lavrov, A. N. Electrical resistivity anisotropy from self-organized one dimensionality in high-temperature superconductors. *Phys. Rev. Lett.* **88**, 137005 (2002).
- [6] Hinkov, V. *et al.* Electronic liquid crystal state in the high-temperature superconductor  $\text{YBa}_2\text{Cu}_3\text{O}_{6.45}$ . *Science* **319**, 597–600 (2008).
- [7] Daou, R. *et al.* Broken rotational symmetry in the pseudogap phase of a high-Tc superconductor. *Nature* **463**, 519–522 (2010).
- [8] Lawler, M. J. *et al.* Intra-unit-cell electronic nematicity of the high-Tc copper-oxide pseudogap states. *Nature* **466**, 347–351 (2010).
- [9] Cyr-Choinière, O. *et al.* Two types of nematicity in the phase diagram of the cuprate superconductor  $\text{YBa}_2\text{Cu}_3\text{O}_y$ . *Phys. Rev. B* **92**, 224502 (2015).
- [10] Ramshaw, B. J. *et al.* Broken rotational symmetry on the Fermi surface of a high-Tc superconductor. *npj Quantum Mater.* **2** (2017).
- [11] Kivelson, S. A. *et al.* How to detect fluctuating stripes in the high-temperature superconductors. *Rev. Mod. Phys.* **75**, 1201–1241 (2003).
- [12] Vojta, M. Lattice symmetry breaking in cuprate superconductors: stripes, nematics, and superconductivity. *Adv. Phys.* **58**, 699–820 (2009).
- [13] Keimer, B., Kivelson, S. A., Norman, M. R., Uchida, S. & Zaanen, J. From quantum matter to high-temperature superconductivity in copper oxides. *Nature* **518**, 179–186 (2015).
- [14] Fradkin, E., Kivelson, S. A. & Tranquada, J. M. Colloquium: Theory of intertwined orders in high temperature superconductors. *Rev. Mod. Phys.* **87**, 457–482 (2015).
- [15] Kivelson, S. A., Fradkin, E. & Emery, V. J. Electronic liquid-crystal phases of a doped mott insulator. *Nature* **393**, 550 (1998).
- [16] Yamase, H. & Kohno, H. Instability toward formation of quasi-one-dimensional Fermi surface in two-dimensional t-J model. *J. Phys. Soc. Jpn.* **69**, 2151 (2000).
- [17] Kivelson, S. A., Fradkin, E. & Geballe, T. H. Quasi-one-dimensional dynamics and nematic phases in the two-dimensional emery model. *Phys. Rev. B* **69**, 144505 (2004).
- [18] Yamase, H. & Metzner, W. Magnetic excitations and their anisotropy in  $\text{YBa}_2\text{Cu}_3\text{O}_{6+x}$ : Slave-boson mean-field analysis of the bilayer t-J model. *Phys. Rev. B* **73**, 214517 (2006).
- [19] Yamase, H. Theory of reduced singlet pairing without the underlying state of charge stripes in the high-temperature superconductor  $\text{YBa}_2\text{Cu}_3\text{O}_{6.45}$ . *Phys. Rev.*

- B* **79**, 052501 (2009).
- [20] Okamoto, S., Sénéchal, D., Civelli, M. & Tremblay, A.-M. S. Dynamical electronic nematicity from Mott physics. *Phys. Rev. B* **82**, 180511 (2010).
  - [21] Fischer, M. H. & Kim, E.-A. Mean-field analysis of intra-unit-cell order in the emery model of the  $\text{CuO}_2$  plane. *Phys. Rev. B* **84**, 144502 (2011).
  - [22] Andersen, B. M., Graser, S. & Hirschfeld, P. J. Correlation and disorder-enhanced nematic spin response in superconductors with weakly broken rotational symmetry. *Europhys. Lett.* **97**, 47002 (2012).
  - [23] Bulut, S., Atkinson, W. A. & Kampf, A. P. Spatially modulated electronic nematicity in the three-band model of cuprate superconductors. *Phys. Rev. B* **88**, 155132 (2013).
  - [24] Fischer, M. H., Wu, S., Lawler, M., Paramakanti, A. & Kim, E.-A. Nematic and spin-charge orders driven by hole-doping a charge-transfer insulator. *New J. Phys.* **16**, 093057 (2014).
  - [25] Volkov, P. A. & Efetov, K. B. Spin-fermion model with overlapping hot spots and charge modulation in cuprates. *Phys. Rev. B* **93**, 085131 (2016).
  - [26] Wang, Y. & Chubukov, A. Charge-density-wave order with momentum  $(2q, 0)$  and  $(0, 2q)$  within the spin-fermion model: Continuous and discrete symmetry breaking, preemptive composite order, and relation to pseudogap in hole-doped cuprates. *Phys. Rev. B* **90**, 035149 (2014).
  - [27] Schütt, M. & Fernandes, R. M. Antagonistic in-plane resistivity anisotropies from competing fluctuations in underdoped cuprates. *Phys. Rev. Lett.* **115**, 027005 (2015).
  - [28] Nie, L., Maharaj, A. V., Fradkin, E. & Kivelson, S. A. Vestigial nematicity from spin and/or charge order in the cuprates. *Phys. Rev. B* **96**, 085142 (2017).
  - [29] Chatterjee, S., Sachdev, S. & Scheurer, M. S. Intertwining topological order and broken symmetry in a theory of fluctuating spin-density waves. *Phys. Rev. Lett.* **119**, 227002 (2017).
  - [30] Tsuchiizu, M., Kawaguchi, K., Yamakawa, Y. & Kontani, H. Multistage electronic nematic transitions in cuprate superconductors: A functional-renormalization-group analysis. *Phys. Rev. B* **97**, 165131 (2018).
  - [31] Zaanen, J., Sawatzky, G. A. & Allen, J. W. Band gaps and electronic structure of transition-metal compounds. *Phys. Rev. Lett.* **55**, 418–421 (1985).
  - [32] Emery, V. J. Theory of high- $T_c$  superconductivity in oxides. *Phys. Rev. Lett.* **58**, 2794 (1987).
  - [33] Lee, P. A., Nagaosa, N. & Wen, X.-G. Doping a Mott insulator: Physics of high-temperature superconductivity. *Rev. Mod. Phys.* **78**, 17 (2006).
  - [34] Zaanen, J. & Oleś, A. M. Canonical perturbation theory and the two-band model for high- $T_c$  superconductors. *Phys. Rev. B* **37**, 9423 (1988).
  - [35] Kolley, E., Kolley, W. & Tiertz, R. Fourth-order interactions in the canonically transformed d-p model for Cu-O superconductors. *J. Phys. C* **4**, 3517 (1992).
  - [36] Zhang, F. C. & Rice, T. M. Effective Hamiltonian for the superconducting Cu oxides. *Phys. Rev. B* **37**, 3759 (1988).
  - [37] Chakravarty, S., Halperin, B. I. & Nelson, D. R. Two-dimensional quantum Heisenberg antiferromagnet at low temperatures. *Phys. Rev. B* **39**, 2344–2371 (1989).
  - [38] Chubukov, A. V., Sachdev, S. & Ye, J. Theory of two-dimensional quantum heisenberg antiferromagnets with a nearly critical ground state. *Phys. Rev. B* **49**, 11919–11961 (1994).
  - [39] Fernandes, R. M., Chubukov, A. V., Knolle, J., Eremin, I. & Schmalian, J. Preemptive nematic order, pseudogap, and orbital order in the iron pnictides. *Phys. Rev. B* **85**, 024534 (2012).
  - [40] Shraiman, B. I. & Siggia, E. D. Mobile vacancies in a quantum Heisenberg antiferromagnet. *Phys. Rev. Lett.* **61**, 467–470 (1988).
  - [41] Sushkov, O. P. & Kotov, V. N. Theory of incommensurate magnetic correlations across the insulator-superconductor transition of underdoped  $\text{La}_{2-x}\text{Sr}_x\text{CuO}_4$ . *Phys. Rev. Lett.* **94**, 097005 (2005).
  - [42] Gabay, M. & Hirschfeld, P. Incommensurate magnetic phases in doped high  $t_c$  compounds. *Physica C* **162–164**, 823–824 (1989).
  - [43] Náfrádi, B. *et al.* Magnetostriction and magnetostructural domains in antiferromagnetic  $\text{YBa}_2\text{Cu}_3\text{O}_6$ . *Phys. Rev. Lett.* **116**, 047001 (2016).
  - [44] Coldea, R. *et al.* Spin waves and electronic interactions in  $\text{La}_2\text{CuO}_4$ . *Phys. Rev. Lett.* **86**, 5377–5380 (2001).
  - [45] Haug, D. *et al.* Neutron scattering study of the magnetic phase diagram of underdoped  $\text{YBa}_2\text{Cu}_3\text{O}_{6+x}$ . *New J. Phys.* **12**, 105006 (2010).
  - [46] Fernandes, R. M., Chubukov, A. V. & Schmalian, J. What drives nematic order in iron-based superconductors? *Nat. Phys.* **10**, 97–104 (2014).
  - [47] Chu, J.-H., Kuo, H.-H., Analytis, J. G. & Fisher, I. R. Divergent nematic susceptibility in an iron arsenide superconductor. *Science* **337**, 710–712 (2012).
  - [48] Armitage, N. P., Fournier, P. & Greene, R. L. Progress and perspectives on electron-doped cuprates. *Rev. Mod. Phys.* **82**, 2421–2487 (2010).
  - [49] The Supplemental Material contains details on analytical and numerical derivations.

# Supplemental Material for “Enhanced nematic fluctuations near an antiferromagnetic Mott insulator and possible application to high- $T_c$ cuprates ”

Peter P. Orth,<sup>1</sup> Bhilahari Jeevanesan,<sup>2</sup> Rafael M. Fernandes,<sup>3</sup> and Jörg Schmalian<sup>2,4</sup>

<sup>1</sup>*Department of Physics and Astronomy, Iowa State University, Ames, Iowa 50011, USA*

<sup>2</sup>*Institute for Theory of Condensed Matter, Karlsruhe Institute of Technology (KIT), 76131 Karlsruhe, Germany*

<sup>3</sup>*School of Physics and Astronomy, University of Minnesota, Minneapolis, Minnesota 55455, USA*

<sup>4</sup>*Institute for Solid State Physics, Karlsruhe Institute of Technology (KIT), 76131 Karlsruhe, Germany*

(Dated: April 22, 2019)

## CONTENTS

S1. Derivation of $t - J - K$ model Hamiltonian from three-band Hubbard model	12
S1.A. Strong-coupling expansion	13
S1.B. Derivation of biquadratic spin exchange $K_0$ from microscopic Hamiltonian	14
Evaluation of the oxygen density response function $\Pi_{\mathbf{q}}^{\alpha\beta}$ for free oxygen holes	16
S1.C. Analysis of bare biquadratic exchange coupling constant $K_0$	17
S1.D. Derivation of biquadratic exchange $K_0$ including interaction of mobile O holes with Cu spins	18
Evaluation of quadrupolar response for mobile holes interacting with Néel ordered Cu spins	19
S1.E. Renormalization of biquadratic exchange coupling $K$ by quadrupolar oxygen density fluctuations	20
S2. Nematic susceptibility within a soft-spin description of the half-filled $t - J - K$ -model	20
S2.A. Nematic susceptibility $\chi_{\text{nem},0}(r, T)$	21
S2.B. Large- $N$ analysis of the nematic susceptibility	23
S3. Spin-wave treatment of $t - J - K$ model at half-filling	23
S4. Details on the Monte-Carlo simulations	25
References	25

### S1. Derivation of $t - J - K$ model Hamiltonian from three-band Hubbard model

The starting point of a microscopic derivation of the biquadratic spin exchange term in the  $t - J - K$  model in Eq. (1) of the main text is the three-band Hubbard model [1]:  $H = H_0 + H_U + H_V$  with parts

$$H_0 = \sum_{\mathbf{R}_i, \sigma} \left\{ (\epsilon_p - \epsilon_d) n_{i\sigma}^p + t_{pd} \sum_u \left[ (-1)^u d_{i\sigma}^\dagger p_{i+u\sigma} + \text{h.c.} \right] + t_{pp} \sum_{u'} \left[ (-1)^{u'} p_{i+\frac{x}{2}+\frac{y}{2}\sigma}^\dagger p_{i+\frac{x}{2}+u'\sigma} + \text{h.c.} \right] \right\} \quad (\text{S.1})$$

$$H_U = \sum_{\mathbf{R}_i} \left( U_{dd} n_{i\uparrow}^d n_{i\downarrow}^d + \frac{U_{pp}}{2} \sum_{u=\frac{x}{2}, \frac{y}{2}} n_{i+u\uparrow}^p n_{i+u\downarrow}^p \right) \quad (\text{S.2})$$

$$H_V = \sum_{\mathbf{R}_i} \left( V_{pd} \sum_u n_i^d n_{i+u}^p + V_{pp} \sum_{u'} n_{i+\frac{x}{2}}^p n_{i+\frac{x}{2}+u'}^p \right). \quad (\text{S.3})$$

Here,  $d_{i\sigma}^\dagger$  creates a Cu ( $3d_{x^2-y^2}$ ) hole with spin  $\sigma$  at Bravais lattice site  $\mathbf{R}_i$ . The operators  $p_{i+\frac{x}{2}\sigma}^\dagger$  and  $p_{i+\frac{y}{2}\sigma}^\dagger$  create O ( $2p_x$ ) and ( $2p_y$ ) holes in the same unit cell  $\mathbf{R}_i$ , respectively. The vacuum is defined as filled  $\text{Cu}^+$  ( $d^{10}$ ) and  $\text{O}^{2-}$  ( $p^6$ ) states. We define the total number of Cu holes with spin  $\sigma$  in unit cell  $\mathbf{R}_i$  as  $n_{i\sigma}^d = d_{i\sigma}^\dagger d_{i\sigma}$  and the Cu hole density as  $n_i^d = \sum_\sigma n_{i\sigma}^d$ . The corresponding operators for oxygen holes read  $n_{i\sigma}^p = \sum_{u=\frac{x}{2}, \frac{y}{2}} p_{i+u\sigma}^\dagger p_{i+u\sigma}$  and  $n_i^p = \sum_\sigma n_{i\sigma}^p$ . The total number of holes on oxygen orbital  $u = \frac{x}{2}, \frac{y}{2}$  reads  $n_{i+u}^p = \sum_\sigma n_{i+u\sigma}^p$ .

The on-site energies of  $d(p)$  orbitals are denoted  $\epsilon_d(\epsilon_p)$  with  $\Delta = \epsilon_p - \epsilon_d > 0$ . The phase factors in the hopping terms arise from the overlap of orbital wavefunctions (see Fig. 1(b) of the main text) and are given by  $(-1)^u = +1$

for  $u = -\frac{\hat{x}}{2}, \frac{\hat{y}}{2}$ ,  $(-1)^u = -1$  for  $u = \frac{\hat{x}}{2}, -\frac{\hat{y}}{2}$  and  $(-1)^{u'} = +1$  for  $u' = \pm\frac{1}{2}(\hat{x} + \hat{y})$ ,  $(-1)^{u'} = -1$  for  $u' = \pm\frac{1}{2}(\hat{x} - \hat{y})$ . The (unrestricted) sum  $\sum_u$  runs over the four vectors connecting a central Cu site to its four neighboring O sites  $u \in \{\pm\frac{\hat{x}}{2}, \pm\frac{\hat{y}}{2}\}$ , and the sum  $\sum_{u'}$  runs over the four vectors connecting an O  $p_x$  orbital to its four  $p_y$  neighbors  $u' \in \{\pm\frac{1}{2}(\hat{x} \pm \hat{y})\}$ . We consider on-site interactions  $U_{dd}$  and  $U_{pp}$  on both Cu and O sites as well as nearest-neighbor interactions  $V_{pd}$  between Cu and O and  $V_{pp}$  between oxygens.

### S1.A. Strong-coupling expansion

The hierarchy of energy scales suggests a strong-coupling expansion in small  $t_{pd} \ll U_{dd} - \Delta, \Delta$ , which yields a description in terms of localized Cu spins coupled to mobile O holes. Note that in order to derive the biquadratic exchange interaction term  $\propto K$  in Eq. (1) of the main text, one can focus on the case of singly occupied Cu sites, *i.e.*, all holes reside on the oxygen sites. In the strong coupling expansion we follow Ref. 2 (see also Ref. 3) that contains an expansion up to fourth order in  $t_{pd}^4/[\Delta^n(U_{dd} - \Delta)^m]$  with  $n + m = 3$  within this subspace.

At second order one finds a term that renormalizes  $t_{pp}$

$$\tilde{H}_{\text{kin}}^{(2)} = \frac{t_{pd}^2}{2} \left( \frac{1}{\Delta} - \frac{1}{U - \Delta} \right) \sum_{i, \sigma, u_1, u_2} (-1)^{u_1 + u_2} p_{i+u_1, \sigma}^\dagger p_{i+u_2, \sigma}, \quad (\text{S.4})$$

and a Cu-O Kondo-like exchange coupling term

$$H_{dp}^{(2)} = 2t_{pd}^2 \left( \frac{1}{\Delta} + \frac{1}{U - \Delta} \right) \sum_{i, u_1, u_2} (-1)^{u_1 + u_2} \mathbf{s}_{i+u_1, i+u_2} \cdot \mathbf{S}_i. \quad (\text{S.5})$$

Here, we have defined the non-local oxygen spin operators  $\mathbf{s}_{ij} = \frac{1}{2} \sum_{\tau, \tau'} p_{i\tau}^\dagger \boldsymbol{\sigma}_{\tau\tau'} p_{j\tau'}$  with  $\boldsymbol{\sigma} = (\sigma^x, \sigma^y, \sigma^z)$  being a vector of Pauli matrices and the usual local Cu spin operators  $\mathbf{S}_i = \frac{1}{2} \sum_{\tau, \tau'} d_{i\tau}^\dagger \boldsymbol{\sigma}_{\tau\tau'} d_{i\tau'}$ .

Below, we present our results in two complementary cases: in case (i) we take both terms (S.4) and (S.5) fully into account, assuming that the mobile oxygen holes move in the background of antiferromagnetically ordered Cu spins. This case is discussed in detail in Sec. S1.D and the main result is shown in Fig. 2 of the main text. In case (ii) we instead consider undressed oxygen holes, and neglect the terms (S.4) and (S.5). This case is discussed in Sec. S1.B. While the oxygen dispersion and resulting Fermi surface is different for the two cases, our main conclusions regarding the emergence of a biquadratic exchange term  $K \propto \Pi^\eta$  remain unchanged. This shows that this is a generic feature of the model and does not rely on a particular oxygen bandstructure. The quadrupolar oxygen fluctuations increase with increasing oxygen repulsion  $V_{pp}$  in both cases. We thus expect it to become the dominant response for sufficiently large  $V_{pp}$ .

At fourth order, there appear further terms that renormalize the oxygen dispersion and Cu-O Kondo-like exchange terms, similar to those in Eqs. (S.4) and (S.5). We neglect those terms as they are a small correction to the second order terms that we take into account (in case (i)). Another fourth-order term is the well-known Heisenberg Cu-Cu spin exchange term

$$H_J^{(4)} = J \sum_{\langle i, j \rangle} \mathbf{S}_i \cdot \mathbf{S}_j \quad (\text{S.6})$$

with exchange interaction constant  $J = t_{pd}^4 \left( \frac{2}{\Delta^3} + \frac{3}{2\Delta^2(U_{dd} - \Delta)} - \frac{1}{2\Delta(U_{dd} - \Delta)^2} \right)$ . Another fourth order term leads to a small renormalization of the oxygen interaction parameters  $U_{pp}$  and  $V_{pp}$ . We neglect these terms as they do not contain any new physics beyond the bare terms that we fully take into account.

In contrast, and most importantly for our analysis, there also appears a Cu-Cu spin exchange interaction term that depends on the hole occupation number of the intermediate oxygen orbital

$$H_{J'} = -J' \sum_{i, \delta} n_{i+\frac{\delta}{2}}^p \mathbf{S}_i \cdot \mathbf{S}_{i+\delta} \quad (\text{S.7})$$

with  $\delta = \{\pm\hat{x}, \pm\hat{y}\}$  and  $J' = t_{pd}^4 \left( \frac{1}{\Delta^3} + \frac{1}{\Delta^2(U_{dd} - \Delta)} - \frac{1}{\Delta(U_{dd} - \Delta)^2} - \frac{1}{(U_{dd} - \Delta)^3} \right)$ . Note that  $J$  and  $J'$  are of the same order in the limit of large  $U_{dd}$ , where one finds  $\lim_{U_{dd} \rightarrow \infty} J'/J = 1/2$ . As we show in detail below, if one integrates over the fluctuations of the oxygen density, Eq. (S.7) gives rise to the biquadratic spin exchange  $\propto K$ . There also appear

non-local manifestations of this term with  $n_i^p$  being replaced by  $n_{ij}^p = \sum_{\sigma} p_{i\sigma}^{\dagger} p_{j\sigma}$ , which give corrections to  $K$ , but are not the focus of our analysis. Finally, at fourth order there also appears a term that describes the coupling of the non-local spin density on the intermediate oxygen site to the cross product of Cu spins

$$H_{ddp}^{(4)} \propto [-2i \sum_{\langle i,j \rangle, u_1, u_2} \mathbf{s}_{i+u_1, j+u_2} \cdot (\mathbf{S}_i \times \mathbf{S}_j)]. \quad (\text{S.8})$$

This term (S.8) has a form similar to Eq. (S.7) after the replacement  $n_{i+\frac{\hat{x}}{2}}^p \rightarrow s_{i+\frac{\hat{x}}{2}, \sigma}^p$ . It thus leads to a coupling between the Cu spins and the quadrupolar oxygen spin (instead of charge) density fluctuations. While a thorough analysis of this term would be interesting, it is beyond the focus of this work. The term (S.8) is also not directly enhanced by large  $V_{pp}$ . It will therefore not change our main conclusions that the biquadratic  $K$  term is dominant for strong oxygen repulsion  $V_{pp}$ , which is the regime of interest to us. Furthermore, close to the Néel state, where the nematic phase is found experimentally, the term (S.8) is suppressed as the cross product  $\mathbf{S}_i \times \mathbf{S}_j = 0$  vanishes in collinear states (such as the Néel state).

### S1.B. Derivation of biquadratic spin exchange $K_0$ from microscopic Hamiltonian

To consider the effect of charge fluctuations on the oxygen sites, we rewrite the oxygen interaction part of the Hamiltonian  $H_{U_{pp}} + H_{V_{pp}}$  in terms of total  $n_i^p$  and relative oxygen density  $\eta_i$  within unit cell  $\mathbf{R}_i$ :

$$n_i^p = n_{i+\frac{\hat{x}}{2}}^p + n_{i+\frac{\hat{y}}{2}}^p \quad (\text{S.9})$$

$$\eta_i = n_{i+\frac{\hat{x}}{2}}^p - n_{i+\frac{\hat{y}}{2}}^p. \quad (\text{S.10})$$

This allows to write the oxygen-density-dependent interaction between neighboring Cu spins in Eq. (S.7) as

$$H_{J'} = -\frac{J'}{2} \sum_i \left[ \eta_i (\mathbf{S}_i \cdot \mathbf{S}_{i+\hat{x}} - \mathbf{S}_i \cdot \mathbf{S}_{i+\hat{y}}) + \eta_{i-\hat{x}} \mathbf{S}_i \cdot \mathbf{S}_{i-\hat{x}} - \eta_{i-\hat{y}} \mathbf{S}_i \cdot \mathbf{S}_{i-\hat{y}} + n_i^p (\mathbf{S}_i \cdot \mathbf{S}_{i+\hat{x}} + \mathbf{S}_i \cdot \mathbf{S}_{i+\hat{y}}) + \sum_{\delta=\hat{x}, \hat{y}} n_{i-\delta}^p \mathbf{S}_i \cdot \mathbf{S}_{i-\delta} \right] \quad (\text{S.11})$$

Terms describing oxygen interactions on-site ( $U_{pp}$ ) and between nearest-neighbors ( $V_{pp}, V_{pd}$ ) in Eqs. (S.14) and (S.15) take the form

$$H_{U_{pp}} + H_{V_{pp}} + H_{V_{pd}} = \frac{1}{N_L} \sum_{\mathbf{k}} \left[ U_{+, \mathbf{k}} n_{\mathbf{k}}^p n_{-\mathbf{k}}^p - U_{-, \mathbf{k}} \eta_{\mathbf{k}} \eta_{-\mathbf{k}} + \frac{V_{pp} f_{\mathbf{k}}}{4} (\eta_{\mathbf{k}} n_{-\mathbf{k}}^p - \eta_{-\mathbf{k}} n_{\mathbf{k}}^p) \right] + 2V_{pd} n_0^p. \quad (\text{S.12})$$

Here, we have performed a Fourier transformation  $\eta_i = \frac{1}{N_L} \sum_{\mathbf{k}} \eta_{\mathbf{k}} e^{i\mathbf{k} \cdot \mathbf{R}_i}$  (and in the same way for  $n_i \rightarrow n_{\mathbf{k}}$ ) with total number of unit cells  $N_L$ . Note that both  $n_i$  and  $\eta_i$  are defined for a Bravais lattice site and denote the mean and difference of the number of oxygen holes in  $p_x$  and  $p_y$  orbitals in the unit cell at Bravais lattice site  $\mathbf{R}_i$ . We perform the Fourier transformation with respect to the Bravais lattice vectors ( $\mathbf{R}_i$ ) not the actual position vectors  $\mathbf{r}_i = \mathbf{R}_i + \mathbf{b}_i$ , where  $\mathbf{b}_i$  refers to the basis vector that denotes the position of the orbital in the unit cell. This is a well-known choice and ensures that the resulting Hamiltonian obeys  $H_{\mathbf{k}+\mathbf{G}} = H_{\mathbf{k}}$  with reciprocal lattice vector  $\mathbf{G}$ . Specifically, we find the following Fourier transformations

$$\eta_i \equiv \eta(\mathbf{R}_i) = \frac{1}{N_L} \sum_{\mathbf{k} \in \text{BZ}} e^{i\mathbf{k} \cdot \mathbf{R}_i} \eta_{\mathbf{k}} \quad (\text{S.13})$$

$$n_{i+\hat{x}/2}^p \equiv n_i^{p,x} = \frac{1}{N_L} \sum_{\mathbf{k} \in \text{BZ}} e^{i\mathbf{k} \cdot \mathbf{R}_i} n_{\mathbf{k}}^{p,x} \quad (\text{S.14})$$

$$n_{i+\hat{y}/2}^p \equiv n_i^{p,y} = \frac{1}{N_L} \sum_{\mathbf{k} \in \text{BZ}} e^{i\mathbf{k} \cdot \mathbf{R}_i} n_{\mathbf{k}}^{p,y}. \quad (\text{S.15})$$

The alternative choice of defining the Fourier transformation with respect to the actual position of the lattice  $\mathbf{r}_i$ , i.e., having  $e^{i\mathbf{k} \cdot (\mathbf{R}_i + \mathbf{b}_i)}$  in the definition of the Fourier transform with  $\mathbf{b}_{d_{x^2-y^2}} = 0$ ,  $\mathbf{b}_{p_x} = \hat{x}/2$  and  $\mathbf{b}_{p_y} = \hat{y}/2$ , is related to the one we use by a gauge transformation.

We have also introduced the interactions  $U_{\pm, \mathbf{k}} = \frac{V_{pp} f_{\mathbf{k}}}{4} \pm \frac{U_{pp}}{8}$ , where the lattice function reads  $f_{\mathbf{k}} = \sum_{\delta'} e^{-i\mathbf{k} \cdot \delta'} = 1 + e^{-ik_x} + e^{ik_y} + e^{i(k_y - k_x)}$ . Here,  $\delta' \in \{0, \hat{x}, -\hat{y}, \hat{x} - \hat{y}\}$  denotes Bravais lattice vectors pointing to unit cells containing



the four nearest-neighbor  $p_y$  oxygen orbitals of a given oxygen  $p_x$  orbital. We note that for simplicity we neglect Eqs. (S.4) and (S.5) here and in the following of this subsection (case (ii) introduced above). We will reinstate the interactions between mobile holes and the localized Cu spins in the derivation presented in Sec. S1.D.

Let us briefly note that the oxygen interaction Hamiltonian in Eq. (S.12) is invariant under the spatial symmetries of the system. In particular, it is invariant under fourfold  $C_4$  rotation  $C_4(x_i, y_i) = (-y_i, x_i)$ ,  $C_4(k_x, k_y) = (-k_y, k_x)$ . This follows from the transformation laws of the orbitals  $p_{i+\frac{x}{2}} \xrightarrow{C_4} p_{C_4(i)+\frac{y}{2}}$  and  $p_{i+\frac{y}{2}} \xrightarrow{C_4} p_{C_4(i)-\frac{x}{2}}$ . The transformation laws for total and relative densities follow as  $\eta_{\mathbf{k}} \xrightarrow{C_4} \frac{1}{2}(1 - e^{-ik_x})n_{\mathbf{k}}^p - \frac{1}{2}(1 + e^{-ik_x})\eta_{\mathbf{k}}$  and  $n_{\mathbf{k}}^p \xrightarrow{C_4} \frac{1}{2}(1 + e^{-ik_x})n_{\mathbf{k}}^p + \frac{1}{2}(e^{-ik_x} - 1)\eta_{\mathbf{k}}$ . Noting that  $f_{\mathbf{k}} \xrightarrow{C_4} f_{C_4^{-1}(\mathbf{k})} = 1 + e^{-ik_y} + e^{-ik_x} + e^{-i(k_y+k_x)} = e^{-ik_y} f_{\mathbf{k}}$ , one can easily show using  $e^{i(k_x-k_y)} f_{\mathbf{k}} = f_{-\mathbf{k}}$  that Eq. (S.12) is invariant under  $C_4$  rotations.

Since the operators  $\eta_{\mathbf{k}}$  and  $n_{\mathbf{k}}^p$  transform into each other under symmetry transformations (such as  $C_4$ ), we need to treat them on equal footing when decoupling the interaction terms using a Hubbard-Stratonovich (HS) transformation. We introduce the vector  $v_{\mathbf{k}} = (n_{\mathbf{k}}^p, \eta_{\mathbf{k}})^T$  and write  $H_{U_{pp}} + H_{V_{pp}} = -\sum_{\mathbf{k}, k_x > 0} v_{\mathbf{k}}^\dagger U_{\mathbf{k}}^{-1} v_{\mathbf{k}}$  with interaction matrix

$$U_{\mathbf{k}}^{-1} = \frac{2}{N_L} \begin{pmatrix} -\text{Re } U_{+, \mathbf{k}} & i \frac{V_{pp}}{4} \text{Im } f_{\mathbf{k}} \\ -i \frac{V_{pp}}{4} \text{Im } f_{\mathbf{k}} & \text{Re } U_{-, \mathbf{k}} \end{pmatrix} \rightarrow U_{\mathbf{k}} = \frac{N_L}{2} \frac{1}{\left(\frac{V_{pp}}{4}\right)^2 |f_{\mathbf{k}}|^2 + \left(\frac{U_{pp}}{8}\right)^2} \begin{pmatrix} -\text{Re } U_{-, \mathbf{k}} & i \frac{V_{pp}}{4} \text{Im } f_{\mathbf{k}} \\ -i \frac{V_{pp}}{4} \text{Im } f_{\mathbf{k}} & \text{Re } U_{+, \mathbf{k}} \end{pmatrix}. \quad (\text{S.16})$$

The HS transformation introduces the fields  $\Phi_{\mathbf{k}} = (\psi_{\mathbf{k}}, \phi_{\mathbf{k}})$  and yields the action

$$S_{U_{pp}+V_{pp}} = \int_{\mathbf{k}} (\Phi_{\mathbf{k}}^\dagger U_{\mathbf{k}} \Phi_{\mathbf{k}} - \Phi_{\mathbf{k}}^\dagger v_{\mathbf{k}} - v_{\mathbf{k}}^\dagger \Phi_{\mathbf{k}}), \quad (\text{S.17})$$

where  $k = (ik_n, \mathbf{k})$  combines Matsubara frequency  $ik_n = 2\pi nT$  with temperature  $T$  and momentum  $\mathbf{k}$ . We note that the fields  $\Phi_{\mathbf{k}}$  transform identical to  $v_{\mathbf{k}}$  in order that the action remains invariant under all symmetry transformations.

We have arrived at an action that is quadratic in oxygen hole operators. In a next step, we will perform the exact functional integration over these degrees of freedom. We focus on those terms in the action that are relevant for the derivation of the biquadratic exchange interaction  $S = S_0 + S_{U_{pp}+V_{pp}} + S_{J'}$ , which read explicitly

$$S = - \int_{q, \mathbf{k}} \sum_{u, u', \sigma, \sigma'} p_{qu\sigma}^\dagger G_{qu\sigma, ku'\sigma'}^{-1} p_{ku'\sigma'} + \int_{\mathbf{k}} \Phi_{\mathbf{k}}^\dagger U_{\mathbf{k}} \Phi_{\mathbf{k}}, \quad (\text{S.18})$$

where  $u, u' \in \{x, y\}$  label  $(p_x, p_y)$  orbitals and  $\sigma, \sigma' \in \{\uparrow, \downarrow\}$  denote the spin direction. The inverse Green's function  $G^{-1}(\mathbf{S}_i)$  in Eq. (S.18) contains the Cu spin operators  $\mathbf{S}_i$  and is a sum of terms

$$G^{-1} = G_0^{-1} + G_{U_{pp}+V_{pp}}^{-1} + G_{J'}^{-1} \quad (\text{S.19})$$

Since all Green's functions are diagonal in spin space,  $G^{-1} \propto \sigma^0$  with  $\sigma^0 = \text{diag}(1, 1)$ , we suppress the spin indices in the following and find

$$G_{0;qu,qu'}^{-1} = (iq_n - \Delta + \mu - 2V_{pd})\tau^0 - t_{pp}\text{Re}(h_{\mathbf{q}})\tau^x + t_{pp}\text{Im}(h_{\mathbf{q}})\tau^y \quad (\text{S.20})$$

$$G_{U_{pp}+V_{pp};qu,ku'}^{-1} + G_{J';qu,ku'}^{-1} = a_{0,q-k}\tau^0 + a_{z,q-k}\tau^z. \quad (\text{S.21})$$

Here,  $\tau^\alpha$  are Pauli matrices in orbital  $(p_x, p_y)$  space,  $\tau^0 = \text{diag}(1, 1)$  and we have defined the lattice function

$$h_{\mathbf{q}} = 1 - e^{iq_x} - e^{-iq_y} + e^{i(q_x - q_y)} \quad (\text{S.22})$$

that describes oxygen hopping. We have also introduced the functions

$$a_{0,q-k} = \psi_{q-k} - \sum_{\mathbf{p}} \mathcal{S}_{\mathbf{p},q-k} h_m(\mathbf{p}, \mathbf{k} - \mathbf{q}) \quad (\text{S.23})$$

$$a_{z,q-k} = \phi_{q-k} - \sum_{\mathbf{p}} \mathcal{S}_{\mathbf{p},q-k} h_\eta(\mathbf{p}, \mathbf{k} - \mathbf{q}). \quad (\text{S.24})$$

These functions contain the HS fields  $\psi_{\mathbf{k}}$  and  $\phi_{\mathbf{k}}$  as well as the spin bilinear  $\mathcal{S}_{\mathbf{p},q} = \mathbf{S}_{\mathbf{p}} \cdot \mathbf{S}_{-\mathbf{p}-q}$ . Under a  $C_4$  rotation it remains invariant  $C_4(\mathcal{S}_{\mathbf{p},q}) = \mathcal{S}_{\mathbf{p},q}$ . The interaction of Cu spins with the intermediate oxygen site [see Eq. (S.11)]

is captured in Fourier space by the lattice functions

$$h_m(\mathbf{p}, \mathbf{k}) = \frac{J'}{2} (e^{ip_x} + e^{ip_y} + e^{-i(p_x+k_x)} + e^{-i(p_y+k_y)}) \quad (\text{S.25})$$

$$h_\eta(\mathbf{p}, \mathbf{k}) = \frac{J'}{2} (e^{ip_x} - e^{ip_y} + e^{-i(p_x+k_x)} - e^{-i(p_y+k_y)}) . \quad (\text{S.26})$$

Functional integration over  $p_{qu\sigma}^\dagger$  and  $p_{qu\sigma}$  yields the action

$$S = \int_k \Phi_k^\dagger U_k \Phi_k - \text{Tr} \log(-G^{-1}) = \int_k \Phi_k^\dagger U_k \Phi_k + \frac{1}{2} \text{Tr}[\{G_0(G_{U_{pp}+V_{pp}}^{-1} + G_{J'}^{-1})\}^2] + \dots \quad (\text{S.27})$$

where the ellipsis stands for the zeroth, first and higher order terms. Focusing on the quadratic term, we write it as

$$S_2 = \frac{1}{2} \text{Tr}[\{G_0(G_{U_{pp}+V_{pp}}^{-1} + G_{J'}^{-1})\}^2] = -\frac{1}{2} \int_q \sum_{\alpha, \beta \in \{0, z\}} a_{\alpha, q} a_{\beta, -q} \Pi_{-q}^{\alpha\beta}, \quad (\text{S.28})$$

where we have introduced the response functions

$$\Pi_q^{\alpha\beta} = - \int_k \text{Tr}[G_{0, k}(\tau^\alpha \sigma^0) G_{0, k+q}(\tau^\beta \sigma^0)] . \quad (\text{S.29})$$

*Evaluation of the oxygen density response function  $\Pi_q^{\alpha\beta}$  for free oxygen holes*

As we show below, the response function  $\Pi^{zz}$  determines the biquadratic exchange coupling  $K_0$ . Here, we investigate the response for free mobile O holes using the Green's function defined in Eq. (S.20). In Sec. S1.D, we evaluate this response function in the opposite regime using a model that includes the interaction of the mobile holes with the antiferromagnetic background of Cu spins (case (ii)). Our results for  $K_0$  are qualitatively the same in both cases, which proves that the emergence and qualitative behavior of  $K_0$  is a generic feature of the underlying three-band Hubbard model defined in Eqs. (S.13)-(S.15).

Let us now explicitly evaluate the different components of the density-density response function  $\Pi_q^{\alpha\beta}$  using the dispersion of free mobile O holes (see Eq. (S.20)). Performing the summation over Matsubara frequencies and setting the external frequency  $iq_n$  to zero, they read

$$\Pi_q^{00} = \int_k \frac{2}{\epsilon_{\mathbf{k}+\mathbf{q}}^2 - \epsilon_{\mathbf{k}}^2} \left\{ \frac{\epsilon_{\mathbf{k}}^2 + g_{+, \mathbf{k}, \mathbf{q}}}{\epsilon_{\mathbf{k}}} [n_F(\tilde{\Delta} + \epsilon_{\mathbf{k}}) - n_F(\tilde{\Delta} - \epsilon_{\mathbf{k}})] - \frac{\epsilon_{\mathbf{k}+\mathbf{q}}^2 + g_{+, \mathbf{k}, \mathbf{q}}}{\epsilon_{\mathbf{k}+\mathbf{q}}} [n_F(\tilde{\Delta} + \epsilon_{\mathbf{k}+\mathbf{q}}) - n_F(\tilde{\Delta} - \epsilon_{\mathbf{k}+\mathbf{q}})] \right\} \quad (\text{S.30})$$

$$\Pi_q^{z0} = \int_k \frac{2g_{-, \mathbf{k}, \mathbf{q}}}{\epsilon_{\mathbf{k}+\mathbf{q}}^2 - \epsilon_{\mathbf{k}}^2} \left\{ \frac{n_F(\tilde{\Delta} + \epsilon_{\mathbf{k}}) - n_F(\tilde{\Delta} - \epsilon_{\mathbf{k}})}{\epsilon_{\mathbf{k}}} - \frac{n_F(\tilde{\Delta} - \epsilon_{\mathbf{k}+\mathbf{q}}) - n_F(\tilde{\Delta} - \epsilon_{\mathbf{k}+\mathbf{q}})}{\epsilon_{\mathbf{k}+\mathbf{q}}} \right\} \quad (\text{S.31})$$

$$\Pi_q^{zz} = \int_k \frac{2}{\epsilon_{\mathbf{k}+\mathbf{q}}^2 - \epsilon_{\mathbf{k}}^2} \left\{ \frac{\epsilon_{\mathbf{k}}^2 - g_{+, \mathbf{k}, \mathbf{q}}}{\epsilon_{\mathbf{k}}} [n_F(\tilde{\Delta} + \epsilon_{\mathbf{k}}) - n_F(\tilde{\Delta} - \epsilon_{\mathbf{k}})] - \frac{\epsilon_{\mathbf{k}+\mathbf{q}}^2 - g_{+, \mathbf{k}, \mathbf{q}}}{\epsilon_{\mathbf{k}+\mathbf{q}}} [n_F(\tilde{\Delta} + \epsilon_{\mathbf{k}+\mathbf{q}}) - n_F(\tilde{\Delta} - \epsilon_{\mathbf{k}+\mathbf{q}})] \right\}, \quad (\text{S.32})$$

and  $\Pi_q^{0z} = -\Pi_q^{z0}$ . Here,  $n_F(x) = [\exp(x/T) + 1]^{-1}$  is the Fermi function and we have defined  $\tilde{\Delta} = \Delta - \mu$ ,  $\epsilon_{\mathbf{q}} = t_{pp}|h_{\mathbf{q}}|$  and  $g_{\pm, \mathbf{q}, \mathbf{k}} = \frac{1}{2} t_{pp}^2 (h_{\mathbf{q}}^* h_{\mathbf{q}+\mathbf{k}} \pm \text{c.c.})$ . We note that the response functions  $\Pi^{\alpha\beta}$  are only  $C_2$  symmetric, but their sum as it appears in the action is always fully  $C_4$  symmetric, which we have verified explicitly. Importantly, in the long wavelength limit, one finds that both  $\lim_{|\mathbf{k}| \rightarrow 0} \Pi^{00} > 0$  and  $\lim_{|\mathbf{k}| \rightarrow 0} \Pi^{zz} > 0$ . This determines the sign of the biquadratic exchange coupling  $K > 0$  as given in Eq. (1) of the main text.

Focusing on the bare biquadratic term arising from the product of the operators  $\mathcal{S}_{\mathbf{p}, \mathbf{q}}$  in Eq. (S.28), it is instructive to write it in real space as

$$S_2^{S^2} = -\frac{J'^2}{2} \sum_{i, j} \left\{ \Pi_{ji}^{00} (\mathbf{S}_i \cdot \mathbf{S}_{i+\hat{x}} + \mathbf{S}_i \cdot \mathbf{S}_{i+\hat{y}}) (\mathbf{S}_j \cdot \mathbf{S}_{j+\hat{x}} + \mathbf{S}_j \cdot \mathbf{S}_{j+\hat{y}}) \right. \\ \left. + \Pi_{ji}^{zz} (\mathbf{S}_i \cdot \mathbf{S}_{i+\hat{x}} - \mathbf{S}_i \cdot \mathbf{S}_{i+\hat{y}}) (\mathbf{S}_j \cdot \mathbf{S}_{j+\hat{x}} - \mathbf{S}_j \cdot \mathbf{S}_{j+\hat{y}}) + 4\Pi_{ji}^{z0} (\mathbf{S}_i \cdot \mathbf{S}_{i+\hat{x}}) (\mathbf{S}_j \cdot \mathbf{S}_{j+\hat{y}}) \right\} \quad (\text{S.33})$$

with  $\Pi_{ji} = \int_{\mathbf{q}} e^{-i\mathbf{q} \cdot (\mathbf{R}_j - \mathbf{R}_i)} \Pi_{-\mathbf{q}}$ . The bare biquadratic exchange coupling  $K_0$  follows as

$$K_0 = \frac{J'^2}{2} \Pi_{ii}^{zz} = \frac{J'^2}{2} \int_{\mathbf{q}} \Pi_{\mathbf{q}}^{zz}. \quad (\text{S.34})$$

We note again that the action  $S_2^{\text{S}^2}$  is fully  $C_4$  invariant and the interaction terms that involve spin operators in neighboring unit cells  $i - \hat{x}$  and  $i - \hat{y}$  arise from the off-diagonal components  $\Pi_{ij}^{z0}$ . In Fig. S.1 we show the response functions  $\Pi^{\alpha\beta}$  both in real and momentum space for parameters  $t_{pp} = 1.0$ ,  $n_p = 0.1$ , and temperature  $T = 0.1$ .

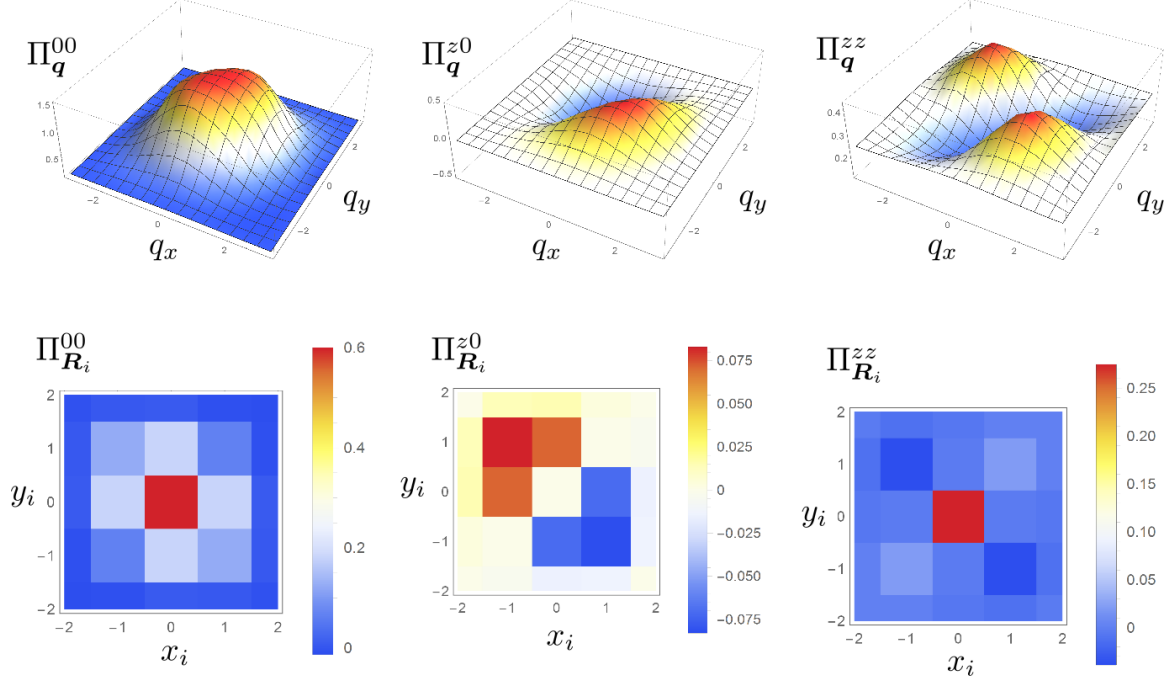


FIG. S.1. Response functions in momentum  $\Pi_{\mathbf{q}}^{\alpha\beta}$  (upper row) and real-space  $\Pi_{i-j}^{\alpha\beta}$  (lower row). From left to right we show  $\Pi^{00}$ ,  $\Pi^{z0}$ ,  $\Pi^{zz}$  for parameters  $t_{pp} = 1.0$ ,  $T = 0.1$ ,  $n_p = 0.1$ . While  $\Pi_{\mathbf{q}}^{\alpha\beta}$  are only  $C_2$ -symmetric, the resulting expression in the action is fully  $C_4$ -symmetric due to multiplication with the lattice functions  $h_m, h_\eta$ . We observe that  $\Pi_{\mathbf{q}}^{zz}$  peaks at a non-zero wavevector showing that the maximal nematic response occurs at a finite  $\mathbf{q}$ .

### S1.C. Analysis of bare biquadratic exchange coupling constant $K_0$

To gain some analytic understanding, we approximate the bare biquadratic coupling constant by

$$K_0 \approx \frac{J'^2}{2} \lim_{\mathbf{q} \rightarrow 0} \Pi_{\mathbf{q}}^{zz} = J'^2 \int_{BZ} \frac{d^2 q}{v_{BZ}} \frac{n_F(\xi_-) - n_F(\xi_+)}{\epsilon_{\mathbf{q}}}. \quad (\text{S.35})$$

Here,  $\xi_{\pm} = \pm \epsilon_{\mathbf{q}} - \mu$  describes the two oxygen bands. Neglecting the interaction with the Néel magnetic background of the localized Cu spins, we obtain the oxygen bandstructure from the lattice function  $h_{\mathbf{q}} = 1 - e^{iq_x} - e^{-iq_y} + e^{i(q_x - q_y)}$ :

$$\epsilon_{\mathbf{q}} = t_{pp} |h_{\mathbf{q}}| = 4t_{pp} \left| \sin \frac{q_x}{2} \right| \left| \sin \frac{q_y}{2} \right|. \quad (\text{S.36})$$

It is useful to introduce the density of states

$$g(\epsilon) = \frac{8}{(2\pi)^2} \int_{\cos^{-1}(1-\tilde{\mu})}^{\pi} dq_x \frac{\|\dot{\boldsymbol{\alpha}}(q_x)\|}{\|\nabla_{\xi} \mathbf{q} = \boldsymbol{\alpha}(q_x)\|} = \frac{8}{(2\pi)^2} \frac{4i}{\tilde{\mu}} \left[ K\left(\frac{4}{\tilde{\mu}^2}\right) - F\left(\frac{1}{2} \cos^{-1}(1-\tilde{\mu}), \frac{4}{\tilde{\mu}^2}\right) \right], \quad (\text{S.37})$$

where  $\tilde{\mu} = \mu/(2t_{pp})$ ,  $\alpha(q_x) = (q_x, q_y(q_x))$  with  $q_y(q_x) = \cos^{-1}\left(\frac{1-\tilde{\mu}^2 - \cos q_x}{1-\cos q_x}\right)$ . The function  $F(x)$  [ $K(x)$ ] is the [complete] elliptic integral of the first kind. We note that the density of states logarithmically diverges as  $\epsilon \rightarrow 0$  due to a van-Hove singularity. We can now analyze the low and high-temperature behavior of the nematic response

$$\Pi_{\mathbf{k} \rightarrow 0, \omega=0}^{zz} = \frac{1}{t_{pp}} \int_0^2 d\epsilon \frac{g(\epsilon)}{\epsilon} \frac{\sinh \frac{\epsilon}{T}}{\cosh \frac{\epsilon}{T} + \cosh \frac{\mu}{T}} = \begin{cases} \frac{g(T)(2-|\mu|)}{t_{pp}} + \frac{e^{-|\mu|/T} \log T}{t_{pp}}, & \text{at low } T \ll 2t_{pp} \\ \frac{1}{2Tt_{pp}}, & \text{at high } T \gg 2t_{pp}, \end{cases} \quad (\text{S.38})$$

where  $2-|\mu| \propto n_p$ . At low temperatures, the response is dominated by the constant term proportional to  $n_p$ . As shown in Fig. S.2 and also in Fig. (2) of the main text (for holes that are interacting with the magnetic background (case (ii) treated below)), the biquadratic exchange thus behaves in the experimentally relevant regime at low  $T \ll 2t_{pp}$  as

$$\frac{K_0}{J} \propto \frac{J^2}{J} \frac{n_p}{t_{pp}}. \quad (\text{S.39})$$

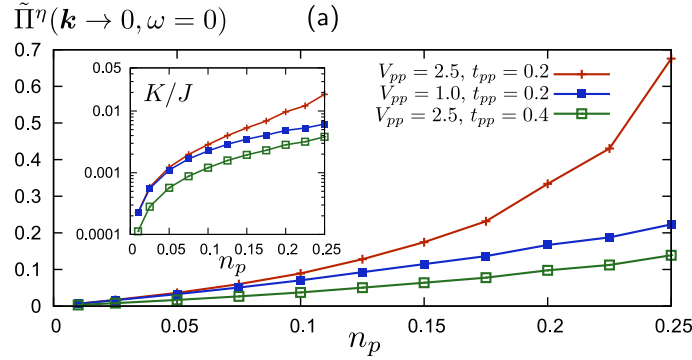


FIG. S.2. Renormalized quadrupolar oxygen density response function  $\tilde{\Pi}_{\mathbf{k}=0}^\eta = \frac{1}{2}[(\Pi_{\mathbf{k}=0}^\eta)^{-1} - U_{\mathbf{k}=0}]$  as a function of oxygen holes  $n_p$  (per planar Cu). Results are obtained for free oxygen dispersion (case (i)) and for parameters  $T = 10^{-2}t_{pp}$ ,  $n_d = 1$ ,  $t_{pd} = 1$ ,  $\Delta = 2.5$ ,  $U_{dd} = 9$ ,  $U_{pp} = 3$ ,  $V_{pd} = V_{pp}$ . Comparing to Fig. (2) of the main text, which is the result for holes interacting with the magnetic background (case (ii)), we find that free oxygen holes exhibit a qualitatively identical, but quantitatively slightly enhanced quadrupolar response (compare values of  $V_{pp}$ ).

#### S1.D. Derivation of biquadratic exchange $K_0$ including interaction of mobile O holes with Cu spins

In this section, we derive the quadrupolar oxygen response  $\Pi_{\mathbf{k}}^\eta$  for the case of mobile oxygen holes that are interacting with a background of Néel ordered Cu spins (case (ii)). The main result of our calculation is presented in Fig. (2) of the main text. This calculation is complementary to our derivation in Sec. for free spins. Since both cases yield qualitatively identical results, this is a strong indication that an enhancement of the quadrupolar response by nearest-neighbor oxygen repulsion  $V_{pp}$  is a generic feature of the model, which does not depend on specific details of the oxygen bandstructure. This is important as the experimental system exhibits nematic order in a regime of the phase diagram with only short-range magnetic order.

The bandstructure of oxygen holes that interact with a background of antiferromagnetically ordered Cu spins is straightforwardly obtained from considering Eqs. (S.4) and (S.5). These terms yield contributions to the oxygen dispersion that depend on the Cu spin state. The resulting four-band model of oxygen holes is diagonal in spin space ( $\sigma = \uparrow, \downarrow$ ) and reads

$$H = \sum_{\mathbf{k}, \sigma} \psi_{\mathbf{k}, \sigma}^\dagger \mathcal{H}_{\mathbf{k}, \sigma} \psi_{\mathbf{k}, \sigma} \quad (\text{S.40})$$

with  $\psi_{\mathbf{k}, \sigma}^\dagger = (p_{x, \mathbf{k}, \sigma}^\dagger, p_{y, \mathbf{k}, \sigma}^\dagger, p_{x, \mathbf{k}+\mathbf{Q}, \sigma}^\dagger, p_{y, \mathbf{k}+\mathbf{Q}, \sigma}^\dagger)$ . The  $4 \times 4$  blocks  $\mathcal{H}_{\mathbf{k}, \sigma}$  in rBZ ( $s = \pm$ ) and orbital ( $\tau = \pm$ ) space read

$$\mathcal{H}_{\mathbf{k}, \sigma} = \begin{pmatrix} \langle \uparrow_s | \tilde{\mathcal{H}}_{\mathbf{k}} | \uparrow_s \rangle & \sigma \langle \uparrow_s | \tilde{\mathcal{H}}_{\mathbf{k}} | \downarrow_s \rangle \\ \sigma \langle \downarrow_s | \tilde{\mathcal{H}}_{\mathbf{k}} | \uparrow_s \rangle & \langle \downarrow_s | \tilde{\mathcal{H}}_{\mathbf{k}} | \downarrow_s \rangle \end{pmatrix} = \begin{pmatrix} \tilde{\mathcal{H}}_{1, \mathbf{k}} & \sigma \tilde{\mathcal{H}}_{2, \mathbf{k}} \\ \sigma \tilde{\mathcal{H}}_{2, \mathbf{k}}^\dagger & \tilde{\mathcal{H}}_{1, \mathbf{k}+\mathbf{Q}} \end{pmatrix}, \quad (\text{S.41})$$

with

$$\tilde{\mathcal{H}}_{1,\mathbf{k}} = \begin{pmatrix} (t_a - t_b) \cos k_x & 2(t_a - t_b - 2t_{pp}) \cos \frac{k_x}{2} \cos \frac{k_y}{2} \\ 2(t_a - t_b - 2t_{pp}) \cos \frac{k_x}{2} \cos \frac{k_y}{2} & (t_a - t_b) \cos k_y \end{pmatrix} \quad (\text{S.42})$$

$$\tilde{\mathcal{H}}_{2,\mathbf{k}} = \begin{pmatrix} i(t_a + t_b) \sin k_x & 2i(t_a + t_b) \cos \frac{k_x}{2} \sin \frac{k_y}{2} \\ 2i(t_a + t_b) \cos \frac{k_x}{2} \sin \frac{k_y}{2} & i(t_a + t_b) \sin k_y \end{pmatrix}. \quad (\text{S.43})$$

*Evaluation of quadrupolar response for mobile holes interacting with Néel ordered Cu spins*

Due to the presence of the antiferromagnetic background of localized Cu spins, the unit cell contains two Cu and four O atoms. The resulting reduced Brillouin zone (rBZ) is thus folded to half its original size. The reciprocal lattice with the reduced zone is spanned by  $\mathbf{Q}_1 = (\pi, \pi)$  and  $\mathbf{Q}_2 = (-\pi, \pi)$ . We are interested in the density-density response function

$$\Pi_{-\mathbf{k}}^{\alpha\beta} = - \int_{q \in \text{rBZ}} \text{Tr} [G_{0,q}(\mathbb{1} \otimes \tau^\alpha) G_{0,q-\mathbf{k}}(\mathbb{1} \otimes \tau^\beta)]. \quad (\text{S.44})$$

Here,  $k = (i\omega_n, \mathbf{k})$  and  $\mathbb{1}$  is a  $4 \times 4$  unit matrix in spin ( $\sigma^\alpha$ ) and folded BZ space ( $+\mathbf{Q}$ , denoted by Pauli matrices  $s^\alpha$ ). As the Hamiltonian is diagonal in spin space, we focus in the following on one of the two spin subspaces, say  $\sigma = \uparrow$ . The trace over spin space simply yields a factor of 2.

The inverse Green's function in orbital/folded BZ space then reads ( $i, j = 1, \dots, 4$ , where  $i = (s, \tau)$ )

$$(G_{0,q}^{-1})_{ij} = (i\omega_n - \Delta + \mu) s^0 \otimes \tau^0 - \mathcal{H}_{q,\sigma=\uparrow(\text{or } \downarrow)}. \quad (\text{S.45})$$

We perform a unitary transformation to band space via  $(\tilde{\mathcal{H}}_{\mathbf{k}})_{ij} = \sum_{m,n} (U_{\mathbf{k}}^\dagger)_{im} (\mathcal{H}_{\mathbf{k}})_{mn} (U_{\mathbf{k}})_{nj} = \epsilon_{i,\mathbf{k}} \delta_{ij}$ , where  $U_{\mathbf{k}}$  contains the eigenvectors as column vectors. The Green's function in band space is diagonal and given by

$$(\tilde{G}_{0,q})_{ij} = U_{\mathbf{q}}^\dagger G_{0,q} U_{\mathbf{q}} = \frac{\delta_{ij}}{i\omega_n - \Delta + \mu - \epsilon_{i,\mathbf{q}}}. \quad (\text{S.46})$$

The quadrupolar density-density response function then takes the form

$$\Pi_{-\mathbf{k}}^{zz} = - \int_q \text{Tr} [G_{0,q}(s^0 \otimes \tau^z) G_{0,q-\mathbf{k}}(s^0 \otimes \tau^z)] = - \int_q \text{Tr} [\tilde{G}_{0,q} V_{\mathbf{q},\mathbf{q}-\mathbf{k}} \tilde{G}_{0,q-\mathbf{k}} V_{\mathbf{q},\mathbf{q}-\mathbf{k}}^\dagger] \quad (\text{S.47})$$

with  $V_{\mathbf{q},\mathbf{q}-\mathbf{k}} = U_{\mathbf{q}}^\dagger (s^0 \otimes \tau^z) U_{\mathbf{q}-\mathbf{k}}$ . We perform the trace, sum over Matsubara frequencies, and set the external frequency to zero (since we are interested in the zero frequency response):

$$\Pi_{-\mathbf{k}}^{zz} = - \int_q \sum_{i,j=1}^4 \left\{ \frac{|(V_{\mathbf{q},\mathbf{q}-\mathbf{k}})_{ij}|^2}{\epsilon_{i,\mathbf{q}} - \epsilon_{j,\mathbf{q}-\mathbf{k}}} \left( n_F(\Delta - \mu + \epsilon_{i,\mathbf{q}}) - n_F(\Delta - \mu + \epsilon_{j,\mathbf{q}-\mathbf{k}}) \right) \right\}. \quad (\text{S.48})$$

We have numerically evaluated this expression in the long-wavelength limit  $|\mathbf{k}| \rightarrow 0$ , where it is useful to explicitly separate the  $i = j$  term

$$\lim_{|\mathbf{k}| \rightarrow 0} \Pi_{-\mathbf{k}}^{zz} = - \int_q \sum_{i \neq j} \frac{|(V_{\mathbf{q},\mathbf{q}-\mathbf{k}})_{ij}|^2}{\epsilon_{i,\mathbf{q}} - \epsilon_{j,\mathbf{q}-\mathbf{k}}} \left( n_F(\Delta - \mu + \epsilon_{i,\mathbf{q}}) - n_F(\Delta - \mu + \epsilon_{j,\mathbf{q}-\mathbf{k}}) \right) - \int_q \sum_{i=1}^4 |(V_{\mathbf{q},\mathbf{q}})_{ii}|^2 \frac{\partial n_F}{\partial \epsilon} (\Delta - \mu + \epsilon_{i,\mathbf{q}}). \quad (\text{S.49})$$

The results of  $\Pi_{-\mathbf{k}}^{zz}$  are presented in Fig. (2) of the main text. Note that an evaluation of the local response (see Eq. (S.34)), which involves a summation over all momenta, is numerically more costly, but differs only by a factor of unity from the long-wavelength result, as we have verified numerically for a number of different system parameters.

### S1.E. Renormalization of biquadratic exchange coupling $K$ by quadrupolar oxygen density fluctuations

We now show that quadrupolar oxygen density fluctuations further enhance the biquadratic spin exchange from its bare value  $K_0$  to a renormalized value  $K > K_0$ . These oxygen density fluctuations become stronger for increasing oxygen-oxygen repulsion  $V_{pp}$ . They are described by the bosonic Hubbard-Stratonovich fields  $\Phi_q = (\psi_q, \phi_q)$  defined above Eq. (S.17). In the parameter regime we consider these fluctuations are non-critical and thus remain massive. Nematic order does not develop spontaneously, but occurs only in the presence of a conjugate symmetry-breaking field such as strain or as provided by the CuO chains in YBCO. After integration over the fermionic fields  $p_{qu\sigma}^\dagger$  and  $p_{qu\sigma}$  the action reads (see Eq. (S.27))

$$S = \int_q \sum_{\alpha, \beta} (\Phi_q^\dagger)_\alpha (U_q)_{\alpha\beta} (\Phi_q)_\beta - \frac{1}{2} \int_q \Pi_q^{\alpha\beta} \left[ (\Phi_q^*)_\alpha - \int_k \mathcal{S}_{k,-q} h_\alpha(\mathbf{k}, \mathbf{q}) \right] \left[ (\Phi_q)_\beta - \int_k \mathcal{S}_{k,q} h_\beta(\mathbf{k}, -\mathbf{q}) \right], \quad (\text{S.50})$$

where  $\alpha, \beta \in \{0, z\}$  and we identify  $h_0(\mathbf{k}, \mathbf{q}) \equiv h_m(\mathbf{k}, \mathbf{q})$  and  $h_z(\mathbf{k}, \mathbf{q}) \equiv h_\eta(\mathbf{k}, \mathbf{q})$ . Performing the Gaussian integration over  $\Phi_q^\dagger$  yields

$$S = S_2^{S^2} - \frac{1}{4} \sum_{\alpha, \beta, \gamma, \gamma'} \int_{q, k_1, k_2} \mathcal{S}_{k_1, q} \mathcal{S}_{k_2, q} h_\gamma(\mathbf{k}_1, -\mathbf{q}) h_{\gamma'}(\mathbf{k}_2, \mathbf{q}) (\tilde{U}_q^{-1})_{\alpha\beta} \Pi_q^{\gamma\alpha} \Pi_q^{\gamma'\beta}, \quad (\text{S.51})$$

where we have defined

$$(\tilde{U}_q)_{\alpha\beta} = (U_q)_{\alpha\beta} - \frac{1}{2} \Pi_q^{\alpha\beta} \quad (\text{S.52})$$

with  $U_q$  given in Eq. (S.16). We note that the action in Eq. (S.51) is fully  $C_4$  symmetric after summation over  $\alpha, \beta, \gamma, \gamma'$ , which we have explicitly verified. We can readily extract the renormalized response functions  $\tilde{\Pi}_q^{\alpha\beta}$  as

$$\tilde{\Pi}_q^{\gamma\gamma'} = \Pi_q^{\gamma\gamma'} + \frac{1}{2} \sum_{\alpha, \beta} (\tilde{U}_q^{-1})_{\alpha\beta} \Pi_q^{\gamma\alpha} \Pi_q^{\gamma'\beta}. \quad (\text{S.53})$$

The renormalized biquadratic exchange interaction is therefore determined by the  $zz$  component  $\tilde{\Pi}_q^{zz} = \Pi_q^{zz} + \frac{1}{2} \sum_{\alpha, \beta} (\tilde{U}_q^{-1})_{\alpha\beta} \Pi_q^{z\alpha} \Pi_q^{z\beta}$ . To gain more insight, we approximate the local response  $\tilde{\Pi}_{ii}^{zz}$ , which determines the biquadratic coupling  $K = \frac{J'^2}{2} \tilde{\Pi}_{ii}^{zz}$  (see Eq. (S.34)), by the  $\mathbf{q} = 0$  component  $\tilde{\Pi}_{\mathbf{q}=0}^{zz}$ . Using that  $(\tilde{U}_{\mathbf{q}=0}^{-1})_{11} = \frac{1}{U_{11} - \frac{1}{2} \Pi_{\mathbf{q}=0}^{zz}}$  with  $U_{11}(\mathbf{q} = 0) = \frac{1}{2} \frac{1}{V_{pp} - \frac{U_{pp}}{8}}$ , the biquadratic exchange  $K$ , renormalized by quadrupolar oxygen density fluctuations, is given by

$$K = \frac{K_0}{1 - (V_{pp} - \frac{U_{pp}}{8}) \Pi_{ii}^{zz}}. \quad (\text{S.54})$$

We show  $K/J$  as a function of hole doping  $n_p$  in Fig. 2(a) of the main text for realistic parameters of the cuprates. The main insight from this result is that while on-site oxygen interactions  $U_{pp}$  tend to reduce the biquadratic exchange, repulsive oxygen-oxygen interactions  $V_{pp}$  enhance the biquadratic spin coupling  $K > K_0$ . For realistic parameters of the cuprates it holds that  $V_{pp} \gg U_{pp}/8$  and the enhancement due to  $V_{pp}$  is the dominant effect.

### S2. Nematic susceptibility within a soft-spin description of the half-filled $t - J - K$ -model

In order to obtain an analytic understanding of the nematic response in the presence of a biquadratic exchange term  $\propto K$  close to a Néel ordered state, we investigate a soft-spin version of the two-dimensional  $t$ - $J$ - $K$ -model at half-filling. We have also analyzed the nematic susceptibility in spatial dimensions  $2 < d \leq 3$  and found that the results for the nematic response from  $d = 2$  remain qualitatively unchanged. After decoupling the biquadratic term at the expense of introducing the Hubbard-Stratonovich field  $\varphi_r$ , the action reads

$$S = \gamma \int_q \left[ r_0 + q^2 + (\varphi_r + h_\varphi)(q_x^2 - q_y^2) + \gamma |\omega_n|^{2/z} \right] M_q^\alpha M_{-q}^\alpha + \frac{\gamma^3 \tilde{u}}{2N} \int_{q_1, q_2, q_3} M_{q_1}^\alpha M_{q_2}^\alpha M_{q_3}^\beta M_{-q_1 - q_2 - q_3}^\beta + \int_r \frac{N \varphi_r^2}{2g}. \quad (\text{S.55})$$



Here,  $\mathbf{M}_q = (M_q^1, M_q^2, \dots, M_q^N)$  with  $q = (i\omega_n, \mathbf{q})$  combining Matsubara frequency  $i\omega_n = 2\pi i n T$  and momentum  $\mathbf{q} = (q_x, q_y)$  denotes the (dimensionless)  $N$ -component staggered Néel magnetization. The integrations run over  $\int_q = T \sum_{\omega_n} \int_{\Lambda} \frac{d^2 q}{(2\pi)^2}$  with dimensionless momentum and frequency cutoffs  $\Lambda$  and  $\gamma\Lambda_\omega$  and  $\int_r = \int_0^\beta d\tau \int d^2 r$ . The coupling constant  $g \propto K/J$  is proportional to the ratio of biquadratic exchange  $K$  to nearest-neighbor Heisenberg exchange  $J$  in the spin model. The (bare) mass parameter  $r_0$  controls the distance to the quantum critical point between Néel ordered and a paramagnetic  $T = 0$  phases, and  $\tilde{u} = u/\gamma$  is a dimensionless interaction constant. We have rescaled the interaction term  $u/N$  to obtain a well-defined large- $N$  limit.

In the following we set the dynamic critical exponent to  $z = 2$ , which describes damping due to particle-hole excitations in the presence of doped holes. We have added a source field  $h_\varphi$  (denoted  $h_r \equiv h_\varphi$  in the main text) that couples to homogeneous nematic order  $\int_x h_\varphi \mathbf{M}_r (\mathbf{M}_{r+\hat{x}} + \mathbf{M}_{r-\hat{x}} - \mathbf{M}_{r+\hat{y}} - \mathbf{M}_{r-\hat{y}})$  with  $\hat{x} = a_0(1, 0)$  and  $\hat{y} = a_0(0, 1)$  with Cu-Cu distance  $a_0$ .

### S2.A. Nematic susceptibility $\chi_{\text{nem},0}(r, T)$

The nematic susceptibility  $\chi_{\text{nem}}(T) = \int_0^{1/T} d\tau \sum_i \langle \mathcal{T}_\tau \varphi_i(\tau) \varphi_0(0) \rangle$  in Eq. (5) of the main text is obtained from the partition function  $Z = \int \mathcal{D}(\mathbf{M}_q, \varphi_r) e^{-S}$  as

$$\chi_{\text{nem}} = \frac{1}{\beta L^2} \frac{\partial^2 \ln Z}{\partial h_\varphi^2} \Big|_{h_\varphi=0} = \frac{\chi_{\text{nem},0}}{1 - \frac{g}{N} \chi_{\text{nem},0}} \quad (\text{S.56})$$

with inverse temperature  $\beta = 1/T$  and bare nematic susceptibility

$$\chi_{\text{nem},0} = \frac{N}{g} - \frac{1}{\beta L^2 \langle \bar{\varphi}_r^2 \rangle}. \quad (\text{S.57})$$

To obtain this expression, we have shifted the field  $\bar{\varphi}_r = \varphi_r + h_\varphi$  in Eq. (S.55) before taking the derivatives with respect to  $h_\varphi$  and assumed the absence of an external field  $h_\varphi = 0$  so that  $\langle \bar{\varphi}_r \rangle^2 = 0$ . We focus on static and homogeneous Hubbard-Stratonovich fields  $\varphi_r$  and  $\bar{\varphi}_r$ , *i.e.*, both fields are independent of  $r$ . To analytically calculate the expectation value  $\langle \bar{\varphi}_r^2 \rangle$ , we decouple the quartic term  $\propto u$  in Eq. (S.55) by defining the (dimensionless) density  $\rho_\psi = \frac{1}{N} \mathbf{M}_x \cdot \mathbf{M}_x$  and introducing a factor of unity as  $1 = \int \mathcal{D}(\rho_\psi, \psi) e^{-\frac{1}{\gamma} \int_r (\mathbf{M}_x^2 - N \rho_\psi) \psi}$  [4], to arrive at

$$S = \gamma \int_q [r_0 + \psi + \mathbf{q}^2 + \bar{\varphi}_r(q_x^2 - q_y^2) + \gamma|\omega_n|] \mathbf{M}_q \cdot \mathbf{M}_{-q} + \frac{N}{\gamma} \int_r \frac{(\bar{\varphi}_r - h_\varphi)^2}{2\tilde{g}} + \frac{N}{\gamma} \int_r \left( \frac{\tilde{u}}{2} \rho_\psi^2 - \psi \rho_\psi \right). \quad (\text{S.58})$$

Here, the dimensionless field  $\psi$  describes the renormalization of the mass from  $r_0 \rightarrow r \equiv r_0 + \psi$ . Separating longitudinal and transverse components  $\mathbf{M}_r = (\sqrt{N}M, \boldsymbol{\pi}_r)$ , where we restrict to homogeneous magnetic order  $M$ , and integrating over the  $(N-1)$  transverse components, we arrive at the action density  $s$ :

$$s \equiv \frac{S}{\beta L^2 \gamma^{-1}} = N(r_0 + \psi)M^2 + \frac{N-1}{2} \gamma \int_q \ln(r_0 + \psi + \mathbf{q}^2 + \bar{\varphi}_r(q_x^2 - q_y^2) + \gamma|\omega_n|) + \frac{N(\bar{\varphi}_r - h_\varphi)^2}{2\tilde{g}} + N \left( \frac{\tilde{u}}{2} \rho_\psi^2 - \psi \rho_\psi \right). \quad (\text{S.59})$$

Next, we expand the logarithm in small  $\bar{\varphi}$  to find

$$\frac{s}{N} = \frac{\gamma}{2} \int_q \log r_q + \frac{\bar{\varphi}_r^2}{2} \left( \frac{1}{\tilde{g}} - \gamma \int_q \frac{q^4 \cos^2(2\theta)}{2r_q^2} \right) + \frac{\tilde{u}}{2} \rho_\psi^2 - \psi \rho_\psi + \mathcal{O}(\bar{\varphi}^3), \quad (\text{S.60})$$

where  $\mathbf{q} = |\mathbf{q}|(\cos \theta, \sin \theta)$  and  $r_q = r + q^2 + \gamma|\omega_n|$  with  $r = r_0 + \psi$ . The generating functional of  $\bar{\varphi}_r$  then reads

$$W[h_\varphi] = \frac{1}{Z} \int \mathcal{D}(\bar{\varphi}_r) e^{-S - \bar{\varphi}_r h_\varphi} = \exp \left[ \frac{h_\varphi^2}{2N} \frac{\gamma}{\beta L^2} \left( \frac{1}{\tilde{g}} - \gamma \int_q \frac{q^4 \cos^2(2\theta)}{2r_q^2} \right)^{-1} \right] \quad (\text{S.61})$$

and the bare nematic susceptibility  $\chi_{\text{nem},0}$  in Eq. (S.57) follows to

$$\chi_{\text{nem},0} = \frac{N}{2} T \sum_{\omega_n} \int_0^\Lambda \frac{d^2 q}{(2\pi)^2} \frac{q^4 \cos^2(2\theta)}{(r + q^2 + \gamma|\omega_n|)^2} = \frac{N}{(2\pi)^2 \gamma} \int_0^{\gamma\Lambda_\omega} d\omega \int_0^\Lambda dq \frac{\omega(r + q^2) q^5}{[(r + q^2)^2 + \omega^2]^2} \coth\left(\frac{\omega}{2\gamma T}\right). \quad (\text{S.62})$$

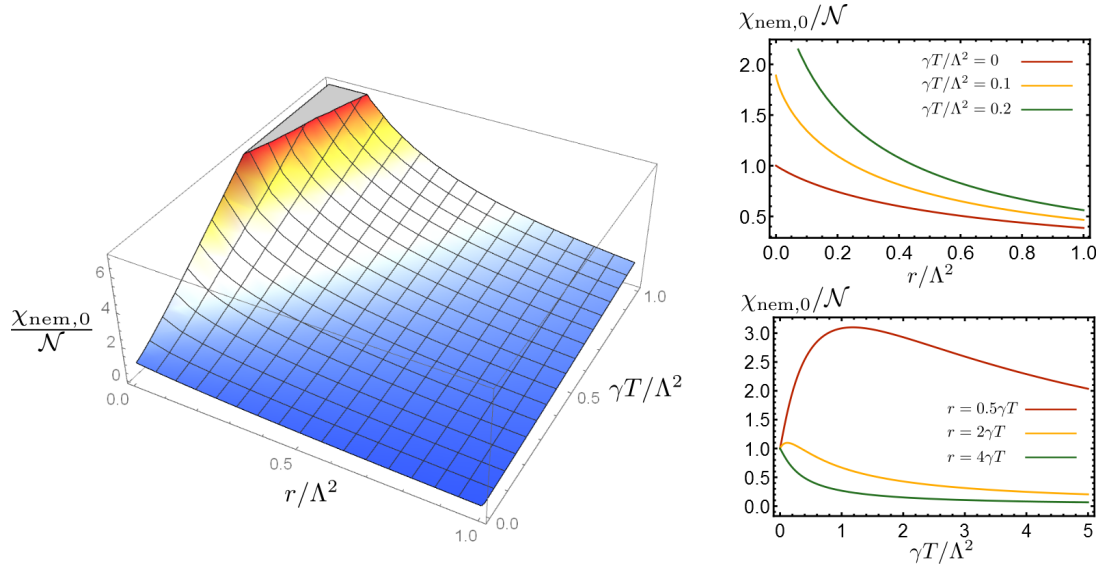


FIG. S.3. (Left) Nematic susceptibility  $\chi_{\text{nem},0}/\mathcal{N}$  with cutoff dependent normalization factor  $\mathcal{N} = N\Lambda^4/(64\pi^2\gamma)$  as a function of  $\tilde{r} = r/\Lambda^2$  and  $\tilde{T} = \gamma T/\Lambda^2$ . We observe that for fixed temperature  $T$ , the susceptibility increases as  $r \propto \xi^{-2}$  decreases (see panel on the upper right). This shows that Néel fluctuations enhance the nematic susceptibility. As a function of temperature, we observe that  $\chi_{\text{nem},0}/\mathcal{N}$  starts out from a non-zero value at  $T = 0$  that is equal to  $\chi_{\text{nem},0}(r = 0, T = 0)/\mathcal{N} = 1$  at the quantum critical point and smaller for  $r > 0$ . The finite-temperature behavior of  $\chi_{\text{nem},0}[r(T), T]/\mathcal{N}$  depends on microscopic details as expected for a non-universal quantity. The panel on the lower right shows the finite- $T$  behavior above the quantum critical point for different values of the slope  $r(T) = a\gamma T$ ,  $a = \{0.5, 2, 4\}$ . For  $a < \pi$  ( $a > \pi$ ) the susceptibility first increases (decreases) linearly as a function of  $T$ , at larger  $T$  it decays to zero. It reaches a maximum when  $\tilde{r} \approx 1$ , which marks the transition into the lattice high- $T$  regime.

In the final step we have gone from summation over Matsubara frequencies to integration along the real frequency axis, and performed the angular integration over  $\theta$ . Note that while  $\omega_n$  has units of energy, the integration variable  $\omega$  is dimensionless by expressing energies in units of  $\gamma^{-1}$ . While we must keep both momentum and frequency cutoff  $\Lambda$  and  $\gamma\Lambda_\omega$  finite when we solve for  $r(r_0, T)$  in the following section (using the large- $N$  approximation), we may take the limit  $\gamma\Lambda_\omega \rightarrow \infty$  in Eq. (S.62). This allows us to exactly perform the momentum and frequency integrations and completely absorb the cutoff  $\Lambda$  by expressing  $\chi_{\text{nem},0}$  in terms of the (dimensionless) variables  $\tilde{r} = r/\Lambda^2$  and  $\tilde{T} = \gamma T/\Lambda^2$  as

$$\chi_{\text{nem},0} = \frac{N\Lambda^4}{64\pi^2\gamma} \left[ 4\pi\tilde{T} \left[ \frac{2\tilde{r}+1}{\tilde{r}+1} + 2\tilde{r} \log \frac{\tilde{r}}{\tilde{r}+1} \right] + 2\psi \left( 1 + \frac{\tilde{r}+1}{2\pi\tilde{T}} \right) - 8\pi\tilde{T} \left\{ \log \Gamma \left( \frac{\tilde{r}+1+2\pi\tilde{T}}{2\pi\tilde{T}} \right) + 2\pi\tilde{T} \left[ \psi^{(-2)} \left( 1 + \frac{\tilde{r}}{2\pi\tilde{T}} \right) - \psi^{(-2)} \left( 1 + \frac{r+1}{2\pi\tilde{T}} \right) \right] \right\} \right]. \quad (\text{S.63})$$

In Fig. S.3, we show  $\chi_{\text{nem},0}/\mathcal{N}$ , where  $\mathcal{N} = N\Lambda^4/(64\pi^2\gamma)$  as a function of  $\tilde{r} = r/\Lambda^2$  and  $\tilde{T} = T/\Lambda^2$ . Note that  $\mathcal{N} \equiv \chi_{\text{nem},0}(r = 0, T = 0)$  is the value of the susceptibility at the quantum critical point. Along a path of constant temperature, the nematic susceptibility increases as  $r$  decreases, which is also shown in the upper right panel of Fig. S.3. Decreasing  $r \propto \xi^{-2}$  implies an increasing magnetic Néel correlation length as one approaches the  $T = 0$  quantum critical point or the renormalized classical regime with exponentially large magnetic correlation length at  $T > 0$ . The nematic susceptibility thus increases as a result of larger magnetic Néel fluctuations. Our analysis also reveals that while for classical spins  $\chi_{\text{nem},0}$  vanishes as  $T \rightarrow 0$ , quantum fluctuations render the zero temperature limit of  $\chi_{\text{nem},0}$  finite.

To plot  $\chi_{\text{nem},0}$  along a path of constant  $r_0$ , which controls the distance to the quantum critical point beyond which Néel order disappears, one needs to solve for the renormalized mass parameter  $r(T, r_0)$ . At finite temperatures above the quantum critical point, one finds  $r(T, r_{0,c}) = a\gamma T \propto T$  with a non-universal proportionality constant  $a$  that depends on microscopic details of the system. As shown in the lower right panel of Fig. S.3, the shape of  $\chi_{\text{nem},0}$  crucially depends on the value of the slope parameter  $a$ , which controls the relative importance of quantum and thermal fluctuations. For small values of  $a < \pi$ ,  $\chi_{\text{nem},0}$  develops a pronounced finite-temperature peak, whose amplitude increases with decreasing  $a$ . This behavior of  $\chi_{\text{nem},0}$  closely resembles the behavior found within the

classical Monte-Carlo simulations (see Fig. 2 of the main text), and show that thermal fluctuations are dominant for  $a < \pi$ . In contrast, for larger values  $a > \pi$ ,  $\chi_{nem,0}$  peaks at  $T = 0$  and is a monotonically decreasing function for finite  $T$ , showing the dominance of quantum fluctuations in this case.

### S2.B. Large- $N$ analysis of the nematic susceptibility

In order to determine the effective mass parameter  $r(T, \delta r_0)$  as a function of temperature  $T$  and distance to the quantum critical point  $\delta r_0 = r_0 - r_{0,c}$ , we consider the limit of large- $N$ , where the partition function is governed by the saddle point of the action in Eq. (S.55). Finding the saddle-point of the action in Eq. (S.59) in the absence of nematic order, leads to the well-known large- $N$  self-consistency equations [4, 5]:  $rM = 0$  with  $r = r_0 + \psi$ ;  $\rho_\psi = \gamma\psi/u$  and

$$r = r_0 + uM^2 + \frac{u}{2} \int_q \frac{1}{r + q^2 + \gamma|\omega_n|} \quad (\text{S.64})$$

The equation requires a finite frequency cutoff  $\Lambda_\omega$ . For the results of  $\chi_{nem,0}$  in Fig. 3 of the main text, we have therefore numerically solved these equations for finite momentum  $\Lambda$  and (dimensionless) frequency cutoffs  $\gamma\Lambda_\omega$ , which yields  $r(r_0, T)$  shown in Fig. S.4. The qualitative behavior of  $\chi_{nem,0}$  as discussed in the previous section does not depend on the exact value of  $\gamma\Lambda_\omega$  and  $\Lambda$  as long as both cutoffs are much larger than  $r, \gamma T \ll \Lambda, \gamma\Lambda$ . The parameters used in Fig. 3 of the main text and Fig. S.4 are for panels (a)  $\delta r_0 = \{-|r_{0,c}|, 0, |r_{0,c}|\}$ , with  $u/\gamma = 50$ ,  $\Lambda = 10$ , and  $\gamma\Lambda_\omega = 100$ ; for panels (b) they are  $\gamma T/\Lambda^2 = \{10^{-6}, 0.1, 0.2\}$ ,  $u/\gamma = 5$ ,  $\Lambda = 10$ , and  $\gamma\Lambda_\omega = 100$ .

### S3. Spin-wave treatment of $t - J - K$ model at half-filling

At half-filling the Hamiltonian in Eq. (1) of the main text describes localized Cu spins interacting via nearest-neighbor Heisenberg exchange interaction  $J$  and a biquadratic exchange interaction  $K$ . Additional weaker next-nearest neighboring and ring-exchange terms may be added to obtain agreement with the experimental spin-wave spectra [6]. Since these terms do not change our conclusions, we do not explicitly consider them below. Note that we include a realistic ferromagnetic exchange coupling  $J_2 = -0.1J$  in our Monte-Carlo simulations (see Fig. 2 of the main text).

We now show that the biquadratic spin exchange term  $\propto K$  does not modify the spin-wave spectrum. Adding such a term in the Hamiltonian is thus fully consistent with previous experimental results of the spin-wave spectrum. We derive our results starting from the  $J$ - $K$  model spin Hamiltonian in Eq. (1) of the main text

$$H = \frac{J}{2} \sum_{i=1}^{N_L} \sum_{\delta_\nu=\delta_1}^{\delta_4} \mathbf{S}_i \mathbf{S}_{i+\delta_\nu} - \frac{K}{4S^2} \sum_{i=1}^{N_L} \left[ \mathbf{S}_i \left( \mathbf{S}_{i+\hat{x}} + \mathbf{S}_{i-\hat{x}} - \mathbf{S}_{i+\hat{y}} - \mathbf{S}_{i-\hat{y}} \right) \right]^2. \quad (\text{S.65})$$

Here,  $\{\delta_\nu\} = \{\pm\hat{x}, \pm\hat{y}\}$  connect nearest-neighbors Cu sites. Let us calculate the spin-wave spectrum around the Néel state. As this corresponds to a large- $S$  limit, we have rescaled the biquadratic term. We follow the standard procedure of Holstein-Primakoff spin-wave calculations [7] and begin with defining local triads  $\mathbf{n}_{1,\mathbf{R}_i} = (\cos(\mathbf{Q} \cdot \mathbf{R}_i), 0, -\sin(\mathbf{Q} \cdot \mathbf{R}_i))$ ,  $\mathbf{n}_2 = (0, 1, 0)$  and  $\mathbf{n}_{3,\mathbf{R}_i} = (\sin(\mathbf{Q} \cdot \mathbf{R}_i), 0, \cos(\mathbf{Q} \cdot \mathbf{R}_i))$  with Néel ordering wavevector  $\mathbf{Q} = (\pi, \pi)$ . Expressing the spins in terms of this local coordinate system  $\mathbf{S}_i = \sum_\alpha \tilde{S}_i^\alpha \mathbf{n}_{\alpha,\mathbf{R}_i}$ , the Hamiltonian takes the form (suppressing the tilde)

$$H = \frac{J}{2} \sum_{i,\delta_\nu,\alpha,\beta} S_i^\alpha S_{i+\delta_\nu}^\beta n_{\beta,\delta_\nu}^\alpha + \frac{K}{4S^2} \sum_i \sum_{\alpha,\beta} \left[ n_{\beta,\delta_\nu}^\alpha S_i^\alpha \left( S_{i+\hat{x}}^\beta + S_{i-\hat{x}}^\beta - S_{i+\hat{y}}^\beta - S_{i-\hat{y}}^\beta \right) \right]^2 \quad (\text{S.66})$$

with  $n_{\beta,\delta_\nu}^\alpha = \delta_{\alpha\beta}(-\delta_{x\alpha} + \delta_{y\alpha} - \delta_{z\alpha})$ . A transformation to momentum space via  $\mathbf{S}_i = \frac{1}{\sqrt{N_L}} \sum_{\mathbf{p} \in BZ} e^{i\mathbf{p} \cdot \mathbf{R}_i} \mathbf{S}_{\mathbf{p}}$  yields

$$H = 2J \sum_{\mathbf{p}} \sum_{\alpha} f_{\mathbf{p}} S_{\mathbf{p}}^\alpha S_{-\mathbf{p}}^\alpha n_{\alpha,\delta_\nu}^\alpha + \frac{K}{N_L S^2} \sum_{\mathbf{p},\mathbf{q},\mathbf{k}} \sum_{\alpha,\beta} S_{\mathbf{p}+\mathbf{k}}^\alpha S_{-\mathbf{p}}^\alpha S_{\mathbf{q}-\mathbf{k}}^\beta S_{-\mathbf{q}}^\beta n_{\alpha,\delta_\nu}^\alpha n_{\beta,\delta_\nu}^\beta (\cos p_x - \cos p_y)(\cos q_x - \cos q_y), \quad (\text{S.67})$$

where we have defined the lattice function  $f_{\mathbf{p}} = \frac{1}{4} \sum_{\delta_\nu} e^{-i\mathbf{p} \cdot \delta_\nu} = \frac{1}{2}(\cos p_x + \cos p_y)$ . To obtain the spin-wave spectrum, we now express spin operators in terms of Holstein-Primakoff bosons  $S_{\mathbf{q}}^x = \sqrt{\frac{S}{2}}(b_{-\mathbf{q}}^\dagger + b_{\mathbf{q}})$ ,  $S_{\mathbf{q}}^y = i\sqrt{\frac{S}{2}}(b_{-\mathbf{q}}^\dagger - b_{\mathbf{q}})$  and

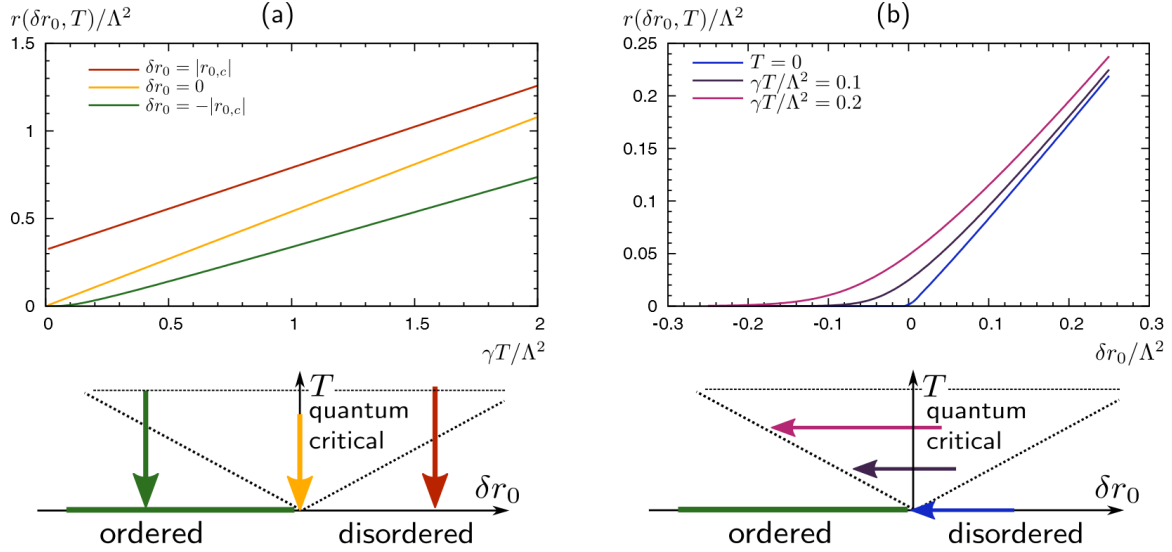


FIG. S.4. Large- $N$  solutions for the “mass” parameter  $r(r_0, T) \propto \xi^{-2}$ , where  $\xi$  is the magnetic correlation length for Néel order. This parameter controls the distance to criticality. The resulting nematic susceptibilities are shown in Fig. 3 of the main text. Panels (a) and (b) correspond to same panels in Fig. 3 of the main text. The left panel (a) shows  $r$  as a function of temperature at fixed distance to criticality  $\delta r_0$ , as depicted in the schematic diagram with vertical paths corresponding to different values of  $\delta r_0$ . For  $\delta r_0 > 0$  (red),  $r$  approaches a finite value as  $T \rightarrow 0$  corresponding to a finite magnetic correlation length in the quantum disordered phase. In contrast, for  $\delta r_0 \leq 0$  (yellow, green),  $r \rightarrow 0$  as  $T \rightarrow 0$ . Approaching the quantum critical point (yellow), one finds  $r = a\gamma T$  with non-universal slope  $a$  that depends among others on the size of the interactions  $u/\gamma$ . Larger  $u/\gamma$  yields a larger  $a$ . Approaching the magnetically ordered phase (green), we observe a change in functional behavior of  $r(T)$  as we cross from the quantum critical to the renormalized classical regime. In the quantum critical regime at higher  $T$ , one finds  $r(T) \propto T$ . In contrast, in the renormalized classical regime at lower  $T$ , it holds  $r(T) \propto T \exp(-\Delta(\delta r_0)/T)$ , where  $\Delta$  depends on the spin stiffness in the ordered phase (rigidity towards magnetic fluctuations) [5]. The right panel (b) corresponds to changing  $\delta r_0$  at fixed temperature  $T$ . In an experiment, this corresponds, for example, to tuning the chemical composition or pressure. Importantly, we observe that  $r \propto \xi^{-2}$  is a monotonously decreasing function for decreasing  $\delta r_0$ , *i.e.*, approaching the quantum critical point or the renormalized classical region. While in two dimensions the Hohenberg-Mermin-Wagner theorem ensures a finite correlation length  $r > 0$  at any finite temperature  $T$ , one finds that  $r(T)$  becomes exponentially small, because  $\xi$  becomes exponentially large, in the renormalized classical regime to the left of the dashed line. From Fig. 2 of the main text, we conclude that the nematic susceptibility  $\chi_{\text{nem}}$  increases if  $r$  decreases or  $\xi$  increases, which shows that larger Néel fluctuations enhance the nematic response.

$S_q^z = \sqrt{N_L} S \delta_{q,0} - \frac{1}{\sqrt{N_L}} \sum_{\mathbf{k}} b_{\mathbf{k}-\mathbf{q}}^\dagger b_{\mathbf{k}}$ . The classical ground state energy follows as the  $\mathcal{O}(S^2)$ -term to  $H^{(S^2)}/(N_L S^2) = -2J$ . Note that the energy of the biquadratic term vanishes in the Néel state.

The next lowest order in  $S$  is quadratic in the bosons and yields upon diagonalization the spin-wave spectrum. Keeping the quadratic terms, yields

$$H_J^{(S)} = 2JS \sum_{\mathbf{q}} \left( 2b_{\mathbf{q}}^\dagger b_{\mathbf{q}} - f_{\mathbf{q}} (b_{-\mathbf{q}}^\dagger b_{\mathbf{q}}^\dagger + b_{\mathbf{q}} b_{-\mathbf{q}}) \right) \quad (\text{S.68})$$

$$H_K^{(S)} = 0, \quad (\text{S.69})$$

Most importantly, according to Eq. (S.69), the biquadratic term does not contribute to the spin-wave spectrum at order  $\mathcal{O}(S)$ . Intuitively, the vanishing of the biquadratic contribution to the spin-wave spectrum follows from the observation that inserting the classical spin state into one of the factors  $\mathbf{S}_i(\mathbf{S}_{i+\hat{x}} + \mathbf{S}_{i-\hat{x}} - \mathbf{S}_{i+\hat{y}} - \mathbf{S}_{i-\hat{y}})$  gives zero, because the term in the brackets vanishes in the Néel state. More explicit, this result can be seen already from Eq. (S.67): to obtain a term of  $\mathcal{O}(S)$  the term in the bracket has to be of order  $S^3$  in order to combine with the prefactor  $K/S^2$  to a term of  $\mathcal{O}(S)$ . There are two possibilities, which both vanish: (i)  $zzzz$  terms, *i.e.*, selecting 3 Kronecker symbols and selecting one term of the form  $\sum_{\mathbf{k}} b_{\mathbf{k}-\mathbf{q}}^\dagger b_{\mathbf{k}}$  (from  $S_q^z$ ). The Kronecker symbols enforce  $\mathbf{p} = \mathbf{q} = \mathbf{k} = 0$  and therefore  $\cos p_x - \cos p_y = 0$  and  $\cos q_x - \cos q_y = 0$ . The other possibility are (ii) terms of the form  $(zzxx + zzyy + xxzz + yyzz)$ , *i.e.*, selecting two Kronecker symbols and two  $S^x, S^y$  terms. The Kronecker symbols give either  $\mathbf{p} = \mathbf{k} = 0$  or  $\mathbf{q} = \mathbf{k} = 0$  and thus one of the cos-terms vanishes:  $\cos p_x - \cos p_y = 0$  or  $\cos q_x - \cos q_y = 0$ .

We finally want to note that at half-filling, where the spin operators  $\mathbf{S}_i = \frac{1}{2} \sum_{\alpha, \beta} d_{i\alpha}^\dagger \boldsymbol{\sigma}_{\alpha\beta} d_{i\beta}$  become regular spin-

1/2 operators, one can transform the biquadratic exchange term into a sum of bilinear spin exchange terms. Such an identity does not hold away from half-filling when there exists a finite number of holes on Cu sites, and one must include the projection operators in the definition of the fermionic operators  $\tilde{d}_{i\alpha}^\dagger = (1 - n_{i\bar{\alpha}})d_{i\alpha}^\dagger$ .

At half-filling, using the well-known relations for spin-1/2 operators  $(\mathbf{S}_i \cdot \mathbf{S}_j)^2 = \frac{3}{16} - \frac{1}{2} \mathbf{S}_i \cdot \mathbf{S}_j$  and  $(\mathbf{S}_i \cdot \mathbf{S}_j)(\mathbf{S}_i \cdot \mathbf{S}_k) = \frac{1}{4} \mathbf{S}_j \cdot \mathbf{S}_k + \frac{i}{2} \mathbf{S}_i \cdot (\mathbf{S}_j \times \mathbf{S}_k)$ , one may rewrite the biquadratic term as a sum of three *bilinear* spin exchange terms such that the spin Hamiltonian in Eq. (S.65) takes the form

$$H = \frac{1}{2} \left( J + \frac{K}{4S^2} \right) \sum_i \sum_\delta \mathbf{S}_i \cdot \mathbf{S}_{i+\delta} + \frac{K}{8S^2} \sum_i \sum_{\delta'} \mathbf{S}_i \cdot \mathbf{S}_{i+\delta'} - \frac{K}{16S^2} \sum_i \sum_{\delta''} \mathbf{S}_i \cdot \mathbf{S}_{i+\delta''}. \quad (\text{S.70})$$

Importantly, Monte-Carlo simulation results for the Hamiltonian (S.70) show the same enhancement of the nematic susceptibility  $\chi_{\text{nem}}$  as a function of  $K$  as results for the Hamiltonian in Eq. (S.65) with the original biquadratic term. Interestingly, there now appears a non-zero contribution of the  $K$ -dependent exchange terms to the spin-wave spectrum. This explicitly shows that using the above spin transformation rules valid for spin-1/2 does not commute with taking the large- $S$  limit to derive the spin-wave spectrum.

#### S4. Details on the Monte-Carlo simulations

The Monte Carlo simulations were carried out at 100 equally spaced temperature points in the interval  $0.001 < T/J < 2.971$ . We applied a combination of single-move Metropolis Monte Carlo steps and non-local parallel-tempering-exchange steps between neighboring temperature configurations. The simulations shown in Fig. 2 of the main text were carried out for systems of  $40 \times 40$  spins and biquadratic exchange couplings  $K/J = \{0.0, 0, 35, 0.45\}$ . We consider a ferromagnetic next-nearest-neighbor exchange coupling  $J_2 = -0.1J$  as well. Note that the ground state phase transition in the classical model between Néel and collinear order occurs at  $J/2 = J_2 + K$ . Following thermalization, the averages were computed for each temperature with at least  $4.5 \times 10^6$  Monte Carlo sweeps (MCS). The error bars were estimated by using the well-known Jackknife procedure.

- 
- [1] V. J. Emery, *Phys. Rev. Lett.* **58**, 2794 (1987).
  - [2] E. Kolley, W. Kolley, and R. Tiertz, *J. Phys. C* **4**, 3517 (1992).
  - [3] J. Zaanen and A. M. Oleś, *Phys. Rev. B* **37**, 9423 (1988).
  - [4] J. Zinn-Justin, *Quantum Field Theory and Critical Phenomena* (Oxford University Press, New York, NY, USA, 2002).
  - [5] S. Sachdev, *Quantum Phase Transitions* (Cambridge University Press, Cambridge, U.K., 1999).
  - [6] R. Coldea, S. M. Hayden, G. Aeppli, T. G. Perring, C. D. Frost, T. E. Mason, S.-W. Cheong, and Z. Fisk, *Phys. Rev. Lett.* **86**, 5377 (2001).
  - [7] A. Auerbach, *Interacting Electrons and Quantum Magnetism* (Springer-Verlag, New York, 1994).